THE CROSS-CORRELATION BETWEEN GALAXIES OF DIFFERENT LUMINOSITIES AND COLORS

YU WANG^{1,3}, XIAOHU YANG^{1,3}, H.J. Mo², FRANK C. VAN DEN BOSCH⁴ Draft version May 26, 2019

ABSTRACT

We study the cross-correlation between galaxies of different luminosities and colors, using a sample of 284489 galaxies selected from the Sloan Digital Sky Survey, Data Release 4. Galaxies are divided into 6 samples according to luminosity, and each of these samples is further divided into red and blue subsamples according to their (g-r) colors. Projected auto-correlation is estimated for each subsample, and projected cross-correlation is estimated for each pair of subsamples. At projected separations $r_p \gtrsim 1 h^{-1} \text{Mpc}$, all correlation functions are roughly parallel, although the correlation amplitude depends systematically on both luminosity and color. On $r_p \lesssim 1 \, h^{-1}{\rm Mpc}$, the auto- and cross-correlation functions of red galaxies are significantly enhanced relative to the corresponding power laws obtained on larger scales. Such enhancement is absent for blue galaxies and in the crosscorrelation between red and blue galaxies. We estimate the relative bias factor on scales $r \gtrsim 1 \,h^{-1}{\rm Mpc}$ for each subsample using its auto-correlation function as well as its cross-correlation functions with other subsamples. The relative bias factors obtained from different methods are similar. For blue galaxies the luminosity-dependence of the relative bias is strong over the entire luminosity range probed $(-23.0 < M_r \le -18.0)$, while for red galaxies the dependence is weaker and becomes insignificant for luminosities below L^* . In order to examine whether a significant stochastic/nonlinear component exists in the bias relation, we study the ratio $\mathcal{R}_{ij} \equiv W_{ii}W_{jj}/W_{ij}^2$, where W_{ij} is the projected correlation between subsample 'i' and 'j'. We find that the values of \mathcal{R}_{ij} are all consistent with 1 for all-all, redred and blue-blue samples, however significantly larger than 1 for red-blue samples. For faint red faint blue samples the values of \mathcal{R}_{ij} are as high as ~ 2 on small scales $(r_p \lesssim 1 \, h^{-1} \mathrm{Mpc})$ and decrease with increasing r_p . These results suggest that a significant stochastic/nonlinear component exists in the relationship between red and blue galaxies, particularly on small scales.

Subject headings: large-scale structure of the universe - galaxies: halos - methods: statistical

1. INTRODUCTION

In the current scenario of structure formation, galaxies are assumed to form in the cosmic density field through a series of physical processes, such as non-linear gravitational collapse, gas cooling and star formation. In this scenario the distribution of galaxies in space is expected to trace the underlying density field to some degree, but the relationship is not expected to be perfect, because many of the processes involved in galaxy formation can complicate the relationship between galaxies and the dark matter density field. Thus, the study of galaxy clustering in space is an important step both in understanding the mass distribution in the universe, and in understanding how galaxies form in the cosmic density field. The statistical tool commonly adopted to quantify galaxy clustering in space is the correlation functions of galaxies (Peebles 1980). During the last two decades, many authors have estimated the two-point correlation functions of galaxies using various redshift catalogs, to study how galaxy clsutering depends on the properties of galaxies, such as luminosity (e.g. Börner, Mo & Zhou 1989; Park et al. 1994; Loveday et al. 1995; Guzzo et al.

1997; Benoist et al. 1996; Norberg et al. 2001; Zehavi et al. 2002; Zehavi et al. 2005; Li et al. 2006), color (e.g. Willmer et al. 1998; Brown et al. 2000; Zehavi et al. 2002; Zehavi et al. 2005; Li et al. 2006), spectral type (Norberg et al. 2002; Budavari et al. 2003; Madgwick et al. 2003), morphological type (e.g. Jing, Mo & Börner 1991; Guzzo et al. 1997; Willmer et al. 1998; Zehavi et al. 2002; Goto et al. 2003), stellar mass, stellar surface mass density and concentration (Li et al. 2006). All these analyses show that galaxies of different properties may have different distributions in space, indicating that galaxies are biased tracers of the underlying density field and that one has to be careful when using the observed galaxy distribution to infer the mass distribution in the universe.

The observed correlation functions of galaxies can provide important constraint on the relationship between galaxies and dark matter halos, as is demonstrated clearly in the recent halo-occupation and conditionalluminosity-function models (Jing, Mo & Börner 1998; Seljak 2000; Peacock & Smith 2000; Berlind & Weinberg 2002; Cooray & Sheth 2002; Yang, Mo & van den Bosch 2003; van den Bosch, Yang & Mo 2003). With accurate measurements of the clsutering properties for galaxies of different properties, it is now possible to study in great detail how different galaxies occupy different halos and how galaxies trace the cosmic density field.

The correlation analyses carried out so far are mostly based on the auto-correlation function of galaxies. Although such analyses can provide important information about how a population of galaxies is distributed

¹ Shanghai Astronomical Observatory, the Partner Group of MPA, Nandan Road 80, Shanghai 200030, China

² Department of Astronomy, University of Massachusetts,

Amherst MA 01003-9305

Joint Institute for Galaxy and Cosmology (JOINGC) of Shanghai Astronomical Observatory and University of Science and Technology of China

⁴ Max-Planck Institute for Astronomy, D-69117 Heidelberg, Ger-

in space, they do not tell us anything about the relationship between galaxies of different properties. For example, two populations of galaxies may each be strongly clustered in space and yet be spatially segregated so that the cross-correlation between them is weak. In reality, all populations of galaxies may be biased tracers of the underlying mass distribution, and so they must all be positively correlated in space. However, the amplitude of the cross-correlation between any two populations of galaxies depends not only on the bias factors of these two populations, but also on how well each of them trace the mass density field, i.e. on the stochasticity in the bias relation. Thus, it is important to measure the crosscorrelation functions between galaxies of different properties, so as to quantify the relationships between the spatial distributions of different galaxies.

In this paper, we use galaxy samples constructed from the Sloan Digital Sky Survey Data Release 4 (SDSS-DR4) to measure both the auto-correlation functions for galaxies of different luminosities and colors and the crosscorrelation functions between different galaxies. We compare the shapes of the various correlation functions to check the validity of the assumption of linear bias. For each population of galaxies (i.e. for galaxies within given ranges of luminosity and color), we estimate its relative bias factors using its auto-correlation function as well all its cross-correlation functions with other populations of galaxies. These bias factors are averaged to give a mean bias factor for each population, and compared among themselves to constrain possible stochastic/nonliner component in the bias relation. This paper is organized as follows. In section 2, we describe the galaxy samples to be used and how random samples are constructed. In section 3, we describe our method for estimating the correlation functions. Our results about the luminosity- and color-dependence of the correlation functions are presented in Sections 4 and 5, respectively. In Section 6 we discuss the implications of our results for the possible existence of stochastic/non-linear bias in galaxy distribution. Finally, we summarize our findings in Section 7.

Throughout this paper, galaxy distances are obtained from redshifts assuming a cosmology with $\Omega_{\rm m,0}=0.3,~\Omega_{\Lambda,0}=0.7.$ Distances are quoted in units of $h^{-1}{\rm Mpc}$, and absolute magnitudes are quoted in terms of $M+5\log h$, i.e. with h set to be 1, where $h=H_0/(100{\rm kms}^{-1}{\rm Mpc}^{-1})$.

2. THE DATA

2.1. The SDSS Data Release 4

In this paper we use galaxy samples constructed from the New York University Value-Added Galaxy Catalog (NYU-VAGC, see Blanton et al. 2005). The version of the NYU-VAGC used here is based on the SDSS Data Release 4 (Adelman-McCarthy et al. 2006) which consists of three regions: two in the Northern Galactic Cap (NGC) and one in the Southern Galactic Cap (SGC). We refer the two NGC regions separately as NGCE (which is along the celestial equator) and NGCO (which is off the equator). The SGC contains three stripes: one along the celestial equator, one to the north and one to the south. In this paper, we measure the correlation functions separately for NGCE, NGCO and SGC, and obtain the mean

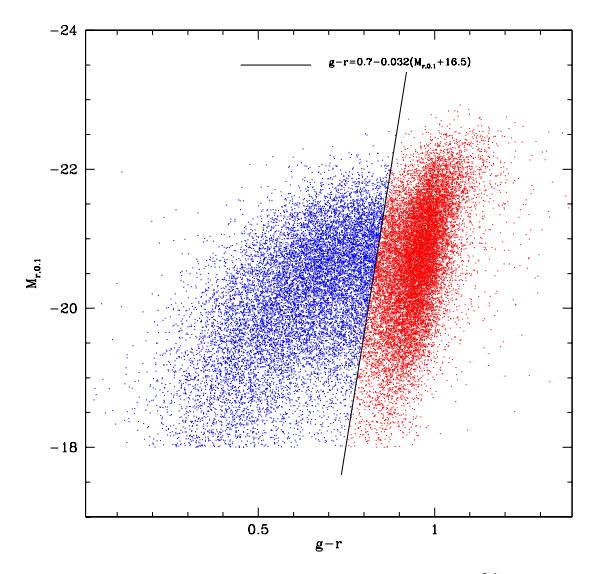


Fig. 1.— The color-magnitude distribution of 10% of the main sample galaxies. The solid line $g-r=0.7-0.032(M_{r,0.1}+16.5)$ separates the galaxies into red and blue populations.

and variance from these samples. Our main sample contains 284489 galaxies with extinction-corrected Petrosian magnitudes in the range 14.5 < r < 17.6, redshifts in the range 0.01 < z < 0.3 and absolute magnitudes in the range $-23.0 < M_{r,0.1} < -18.0$. The r-band absolute magnitudes are corrected to redshift z = 0.1 using the K-correction code of Blanton et al. (2003a) and the luminosity-evolution model of Blanton et al. (2003b). In what follows, all absolute magnitudes and luminosities are quoted with such corrections. In the apparentmagnitude limits adopted here, 14.5 < r < 17.6, the bright end is chosen to avoid incompleteness due to the large angular sizes of galaxies, while the faint end is chosen to match the magnitude limit of the SDSS main galaxy sample. In our analysis, we will also use another apparent-magnitude criterion, 13.0 < r < 17.6 to construct a supplemental sample. This sample has in total 287728 galaxies, about 3239 more than the main sample described above. Most of these additional galaxies are intrinsically bright galaxies with low redshifts, and the use of these galaxies can significantly improve the signal of the cross-correlation function between the brightest and faintest samples by increasing their overlapping volume between them. As we will see below, since we can normalize the cross-correlation function with the random sample constructed according to the faint sample that is complete, and since the incompleteness introduced by including the brightest galaxies is not expected to be correlated with the real structure, the incompleteness should not introduce significant bias in our results.

From our main sample, we first construct 6 volume-limited samples (Samples V1 – V6) in six bins of absolute-magnitue $(M_{r,0.1})$: V1 (-23.0,-21.5], V2 (-21.5,-21.0], V3 (-21.0,-20.5], V4 (-20.5,-20.0], V5 (-20.0,-19.0], V6 (-19.0,-18.0], with detailed selection criteria given in Table 1. Obviously, the redshift overlap between the brightest and faintest samples is small (and sometimes none). In order to enlarge the redshift overlap, which is necessary in order to measure the cross correlations reliably, we also construct 6 volume-limited samples, Va – Vf, from our supplemental sample.

TABLE 1 Volume-limited samples

		es			
Sample	$M_{r,0.1}$	NGCE	NGCO	SGC	Z
V1/Va	(-23.0, -21.5]	4670/5365	8935/10030	2704/3050	(0.10, 0.19)/(0.05, 0.19)
V2/Vb	(-21.5, -21.0]	9288/9485	16978/17442	4777/4919	(0.05, 0.16)/(0.03, 0.16)
V3/Vc	(-21.0, -20.5]	11833/12110	19987/20542	5676/5837	(0.04, 0.13)/(0.02, 0.13)
V4/Vd V5/Ve	(-20.5, -20.0] (-20.0, -19.0]	10842/11158 $6493/6974$	17705/18348 $15462/16073$	5146/5317 $4317/4571$	(0.03, 0.10)/(0.02, 0.10) (0.03, 0.07)/(0.01, 0.07)
V6/Vf	(-19.0, -18.0]	2620/2690	5321/5485	1534/1590	(0.03, 0.04)/(0.01, 0.04)

Note. — Column 1 indicates the sample ID. Column 2 gives the absolute-magnitude range covered by each sample. Columns 3, 4 and 5 list the galaxy number in each sample in the three regions (NGCE, NGCO, SGC) of the SDSS. Column 6 lists the redshift range of each sample. Each sample is a volume-limited in the redshift range it covers. Samples V1 – V6 are for galaxies with r-band apparent magnitudes in the range from 14.5 to 17.6. Samples Va – Vf are constructed from all galaxies with r-band apparent magnitudes in the range from 13.0 to 17.6. The reason for using these two sets of volume-limited samples is given in the main text.

TABLE 2 FLUX-LIMITED SAMPLES

Sample	M	NGCE (Red/Blue)	Number of Galaxies NGCO (Red/Blue)	SGC (Red/Blue)	- z
F1 (F1 _{red} /F1 _{blue}) F2 (F2 _{red} /F2 _{blue}) F3 (F3 _{red} /F3 _{blue}) F4 (F4 _{red} /F4 _{blue}) F5 (F5 _{red} /F5 _{blue}) F6 (F6 _{red} /F6 _{blue}) F*	(-23.0, -21.5] (-21.5, -21.0] (-21.0, -20.5] (-20.5, -20.0] (-20.0, -19.0] (-19.0, -18.0] (-20.7, -20.2]	8817 (5805/3012) 14189 (8259/5930) 19025 (10942/8083) 17214 (9888/7326) 20252 (11103/9149) 5597 (2278/3319) 18444	17012 (11246/5766) 26598 (15478/11120) 33459 (19178/14281) 29037 (16672/12365) 36386 (19719/16667) 12687 (5609/7078) 31714	5108 (3404/1704) 7556 (4418/3138) 9498 (5416/4082) 8329 (4698/3631) 10162 (5423/4739) 3563 (1657/1906) 8975	(0.05, 0.30) (0.04, 0.21) (0.03, 0.17) (0.03, 0.14) (0.02, 0.11) (0.01, 0.07)

Note. — Similar to Table 1 but for flux-limited samples. Here again galaxies with r-band apparent magnitudes in the range from 14.5 to 17.6 are selected. Numbers are listed separatly for all, red and blue galaxies. F^* is a sample of galaxies with luminosities within a 0.5 magnitude bin around L^* .

In addition to the volume-limited samples described above, we also construct 6 flux-limited samples, F1 -F6, in the same six luminosity bins. Each of these samples includes all galaxies in the corresponding absolutemagnitude bin and the details of these samples are given in Table 2. The advantage of using flux-limited samples is that we have more galaxies in each sample, but the drawback is that the samples are not homogeneous in the radial direction, and so the two samples to be crosscorrelated do not occupy exactly the same volume. As we will show below, the results based on the flux-limited samples are very similar to those based on the volumelimited samples. Because of this, we will focus on the flux samples to take advantage of the larger sample sizes. For each of the flux-limited sample, we further divide galaxies into two color subsamples according to their q-rcolors. The dividing line is given by

$$g - r = 0.7 - 0.032(M_{r,0.1} + 16.5),$$
 (1)

where g and r are the g-band and r-band magnitudes that are K-corrected (Blanton et al. 2003a) and E-corrected (Blanton et al. 2003b) to redshift z=0.1. Galaxies with g-r color above (below) this line are called red (blue) galaxies, and the corresponding samples are denoted by $F1_{\rm red} - F6_{\rm red}$ (red subsamples) and $F1_{\rm blue} - F6_{\rm blue}$ (blue subsamples). The selection criteria for these subsample are listed in Table 2. In Fig. 1 we show the color-magnidute relation for a random set of 10% of all galaxies in our main sample, with the solid line indicat-

ing the color separation given by Eq. (1). Note that this color separation is very similar to what were used earlier (e.g. Blanton et al. 2003c; Baldry et al. 2004; Bell et al. 2004; Hogg et al. 2004; Weinmann et al. 2006).

As comparison, we also construct a reference sample, F^* , which includes all galaxies within a 0.5-magnitude bin around L^* . The selection criteria for this sample are listed in the last line of Table 2.

2.2. The random samples

In order to measure the two-point correlation functions, one needs to construct random samples to normalize the galaxy-pair counts. Since we will study the clustering properties separately for all, red and blue galaxies, we need to generate random samples separately for each of them. In general, if we know the luminosity function of galaxies, we can first construct a random sample with the luminosity function and then apply the observational magnitude limits. Unfortunately, we do not have the luminosity functions for the red and blue galaxies defined according to the color criterion described above. Because of this, here we adopt a method proposed in Li et al. (2006), where a random sample is generated by assigning each galaxy in the real sample a random position in the sky while keeping all other properties (i.e., redshift, color, magnitude, etc.) unchanged. The random sample so constructed has exactly the same redshift distribution as the original sample. However, this method is expected to work well only for wide-angle surveys where sky cover-

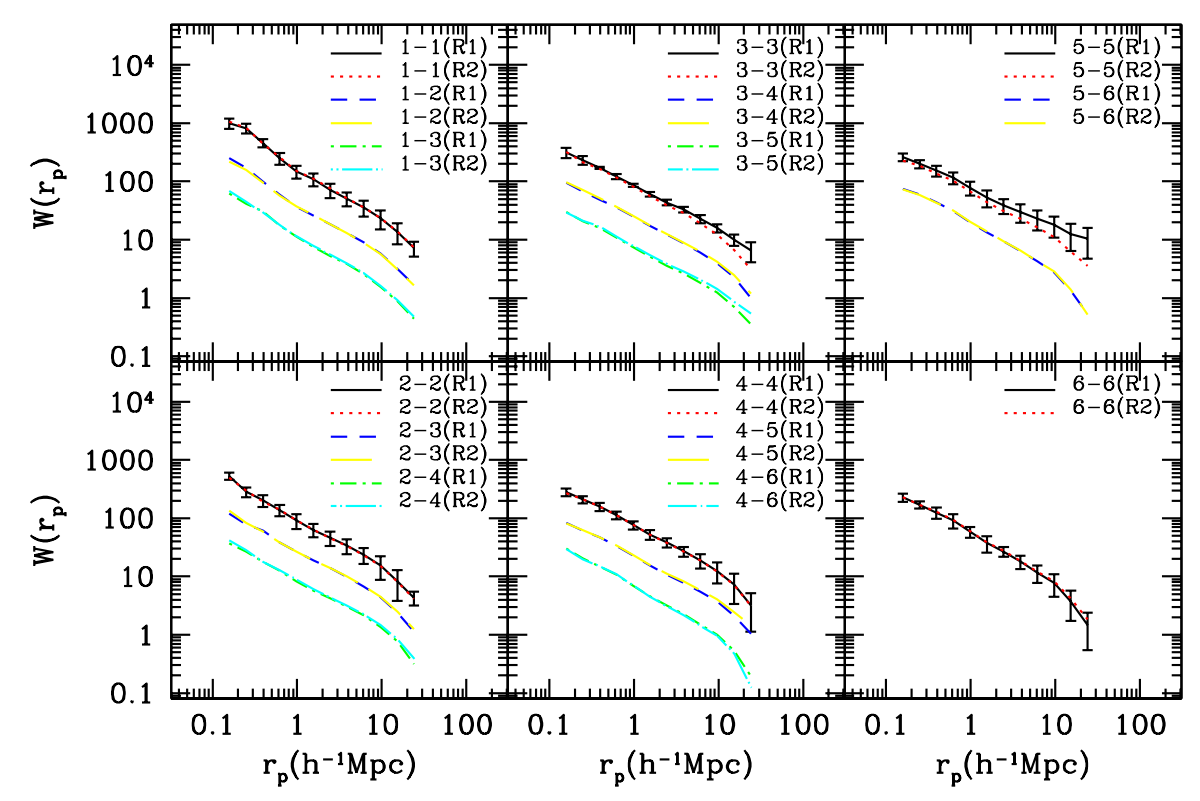


Fig. 2.— The projected 2PCFs for the flux-limited samples. Here we compare the results obtained by using two different random samples, R1 and R2 (see the main text for how R1 and R2 are constructed). The errorbars in this plot represent the 1- σ scatter among the three SDSS regions. For clarity, we only plot errorbars for the auto-correlation functions but note that the errorbars for the cross-correlation functions have similar sizes. The results for the cross-correlation functions are shifted downward by 0.5 and 1 for the cases Fi – F(i+1) and Fi-F(i+2) (i=1,2,3,4,5), respectively. Note that in most of the cases, these two types of random samples yield very similar results. However, discrepancy exists in a few cases, especially for the auto-correlation function of F5. As discussed in the main text, this discrepancy is likely caused by the supercluter at redshift $z \sim 0.08$.

age is much larger than the large-scale structure in question, and requires that the variation in survey depth be small across the sky coverage (Li et al. 2006). The random samples so constructed are referred to as type R1 in the following.

Although Li et al. (2006) found that two-point correlation functions based on the random samples described above match well those obtained using random samples based on the luminosity function, we need to test whether or not the use of different random samples can have significant impact on our results for the smaller subsamples used here. To do this, we generate another set of random samples for all galaxies according to the luminosity function obtained by Blanton et al. (2003b). Here a large set of points are randomly distributed within the survey sky coverage and each point is assigned a redshift and a magnitude according to the luminosity function. This set of random samples will be referred to as type R2.

For both sets of random samples, the *mangle* software provided by A. Hamilton (Hamilton & Tegmark 2004) is used to locate the polygon ID for each random galaxy and to determine the completeness and magnitude limit (which changes slightly across the sky coverage) for this polygon using the mask provided by Blanton et al. (2005). The completeness and magnitude limit so obtained are then included in the random samples.

3. METHOD TO ESTIMATE THE TWO-POINT CORRELATION FUNCTION

We estimate both the 2-point auto- and cross-correlation functions (hereafter 2PCFs) using the definition proposed in Davis & Peebles (1983),

$$\xi_{i,j}(r_p, r_\pi) = \frac{D_i D_j(r_p, r_\pi)}{D_i R_j(r_p, r_\pi)} - 1, \qquad (2)$$

where i, j denote the pair of samples for which the cross correlation function is estimated; i = j corresponds to auto-correlation function. As a convention, sample i always represents the brighter sample if $i \neq j$. In the above definition, D_iD_j is the count of galaxy pairs between samples i and j, $D_i R_j$ is the count of galaxy-random pairs between galaxy sample i and random sample j, and r_p and r_{π} are the separations of galaxy pairs perpendicular and parallel to the line of sight, respectively. Galaxygalaxy and galaxy-random pairs are counted in logarithmic bins in r_p , with bin width $\Delta \log_{10}(r_p) = 0.2$, and in linear bins of r_{π} , with bin width $\Delta r_{\pi} = 1 \, h^{-1} \mathrm{Mpc}$. Since we have galaxy samples in three different regions (NGCE, NGCO and SGC), we combine the number counts of all regions when estimating the mean correlation function. The scatter among the three regions are used to indicate the uncertainties (errorbars) in the measurements.

As mentioned in Section 2.1, the redshift overlap between the brightest and faintest volume-limited samples, V1 and V6, is very small, and we have to use instead samples Va and Vf (which may be incomplete) to get better statistics. According to Eq. (2), one may circumvent the problems to some extent using a combinations of complete and incomplete samples. For example, one

TABLE 3 The correlation lengths and slopes for volume-limited samples on large scales $(0.98\,h^{-1}{\rm Mpc} \le r_p \le 9.6\,h^{-1}{\rm Mpc})$

Sample	Va	Vb	Vc	Vd	Ve	Vf
	α	α	α	α	α	α
	r_0	r_0	r_0	r_0	r_0	r_0
V1	1.84 ± 0.06					
	7.59 ± 0.75					
V2	1.83 ± 0.06	1.77 ± 0.04				
	6.90 ± 0.59	6.11 ± 0.33				
V3	1.85 ± 0.07	1.79 ± 0.06	1.81 ± 0.04			
	6.60 ± 0.64	5.85 ± 0.34	5.62 ± 0.16			
V4	1.82 ± 0.11	1.81 ± 0.08	1.81 ± 0.06	1.80 ± 0.05		
	6.41 ± 0.51	5.67 ± 0.37	5.56 ± 0.25	5.38 ± 0.16		
V5	1.71 ± 0.23	1.79 ± 0.16	1.84 ± 0.13	1.79 ± 0.11	1.83 ± 0.08	
	6.54 ± 0.94	5.23 ± 0.64	5.16 ± 0.40	4.96 ± 0.32	4.90 ± 0.18	
V6					1.86 ± 0.29	1.92 ± 0.30
					4.70 ± 0.43	4.17 ± 0.23
$\alpha = \overline{\alpha} = 1.82$	r_0	r_0	r_0	r_0	r_0	r_0
V1	7.57 ± 0.45					
V2	6.89 ± 0.34	6.13 ± 0.18				
V3	6.56 ± 0.38	5.87 ± 0.20	5.62 ± 0.11			
V4	6.40 ± 0.39	5.67 ± 0.23	5.56 ± 0.14	5.39 ± 0.11		
V5	6.56 ± 0.58	5.26 ± 0.37	5.14 ± 0.29	4.97 ± 0.21	4.89 ± 0.09	
V6					4.65 ± 0.38	4.08 ± 0.20

Note. — The upper part lists the best fit values of r_0 and α for different volume-limited samples, using data points on large scales, $0.98\ h^{-1}{\rm Mpc} \le r_p \le 9.6\ h^{-1}{\rm Mpc}$. The table is not filled up because the overlaps in volume between the faintest and bright samples are too small to allow reliable estimates of the cross correlation functions. The lower part of the table shows the correlation length obtained by setting the slope of the correlation functions, α , to be $\overline{\alpha}=1.82$, the average of the valuese listed in the upper part.

TABLE 4 The correlation lengths and slopes for volume-limited samples on small scales $(0.16\,h^{-1}{\rm Mpc} \le r_p \le 0.98\,h^{-1}{\rm Mpc})$

Sample	Va	Vb	Vc	Vd	Ve	Vf
	α	α	α	α	α	α
	r_0	r_0	r_0	r_0	r_0	r_0
V1	1.89 ± 0.16					
	8.07 ± 0.81					
V2	1.84 ± 0.08	1.86 ± 0.10				
	7.82 ± 0.59	5.77 ± 0.49				
V3	1.83 ± 0.08	1.83 ± 0.06	1.77 ± 0.03			
	7.89 ± 0.66	5.67 ± 0.27	5.71 ± 0.36			
V4	1.82 ± 0.08	1.85 ± 0.08	1.71 ± 0.03	1.71 ± 0.02		
	7.93 ± 0.47	5.61 ± 0.60	5.88 ± 0.56	5.70 ± 0.38		
V5	1.88 ± 0.21	1.96 ± 0.13	1.81 ± 0.09	1.77 ± 0.07	1.72 ± 0.02	
	7.62 ± 0.68	4.90 ± 0.29	5.27 ± 0.38	5.07 ± 0.28	5.27 ± 0.19	
V6					1.80 ± 0.14	1.75 ± 0.13
					4.73 ± 0.36	4.43 ± 0.29
$\alpha = \overline{\alpha} = 1.81$	r_0	r_0	r_0	r_0	r_0	r_0
V1	8.16 ± 0.54					
V2	7.21 ± 0.40	6.00 ± 0.13				
V3	7.07 ± 0.36	5.74 ± 0.12	5.53 ± 0.09			
V4	6.99 ± 0.46	5.76 ± 0.13	5.44 ± 0.08	5.27 ± 0.06		
V5	6.70 ± 0.26	5.45 ± 0.23	5.25 ± 0.12	4.93 ± 0.09	4.90 ± 0.11	
V6					4.69 ± 0.14	4.23 ± 0.09

Note. — The same as Table 3, except that the results are obtained by fitting the correlation functions on small scales, $0.16 \ h^{-1}{\rm Mpc} \le r_p \le 0.98 \ h^{-1}{\rm Mpc}$.

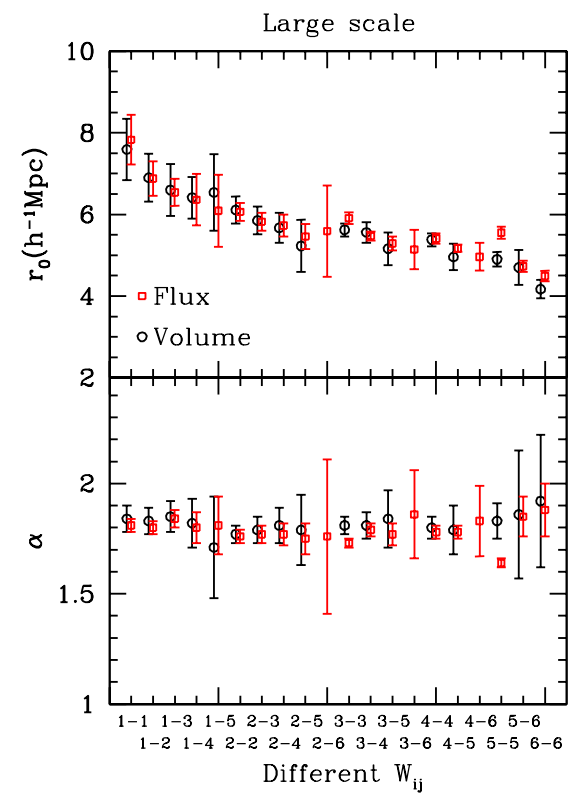


Fig. 3.— The correlation length, r_0 , and logarithmic slope, α , obtained from the projected auto- and cross-correlation functions on scales $0.98\,h^{-1}{\rm Mpc} \le r_p \le 9.6\,h^{-1}{\rm Mpc}$ for various volume-limited and flux-limited samples. The error-bars are 1- σ scatter among the three SDSS regions. In the horizontal axis we indicate the IDs (i-j) of the samples used in the estimate of the correlation function, $W_{i,j}$. The circles with error-bars are the results for volume-limited samples. Overall, the results for volume-limited samples agree well. Large discrepancy exists for $W_{5,5}$, likely due to the existence of the supercluster at redshift $z\sim 0.08$.

can choose the i sample from Va - Vf, and the j sample and the corresponding random sample from V1 - V6. Since V1 - V6 are complete, the effects due to the incompleteness in samples Va - Vf may be reduced.

In our following dscussion, we will focus on the *projected* 2PCF, which is defined as

$$W_{i,j}(r_p) = 2 \int_0^\infty \xi_{i,j}(r_p, r_\pi) dr_\pi = 2 \sum_k \xi_{i,j}(r_p, r_{\pi,k}) \Delta r_{\pi,k} .$$
(3)

Here the summation is made over k=1 to 40 corresponding to $r_{\pi}=0.5~h^{-1}{\rm Mpc}$ to $\pi_{40}=39.5~h^{-1}{\rm Mpc}$. If we assume that the real-space 2PCF $\xi(r)$ can be fitted by a power law,

$$\xi(r) = (r_0/r)^{\alpha} \,, \tag{4}$$

where r_0 and α are, respectively, the correlation length and slope of the correlation function, then the projected 2PCF is related to the real-space 2PCF as

$$W(r_p) = r_0^{\alpha} r_p^{1-\alpha} \frac{\Gamma(1/2)\Gamma[(\alpha-1)/2]}{\Gamma(\alpha/2)}, \qquad (5)$$

where $\Gamma(x)$ is the Gamma function. As we will see below, the observed 2PCFs can all be fitted reasonably well by power laws over limited ranges of r_p . We can then use r_0 to represent the correlation amplitude, and α the shape of the correlation function.

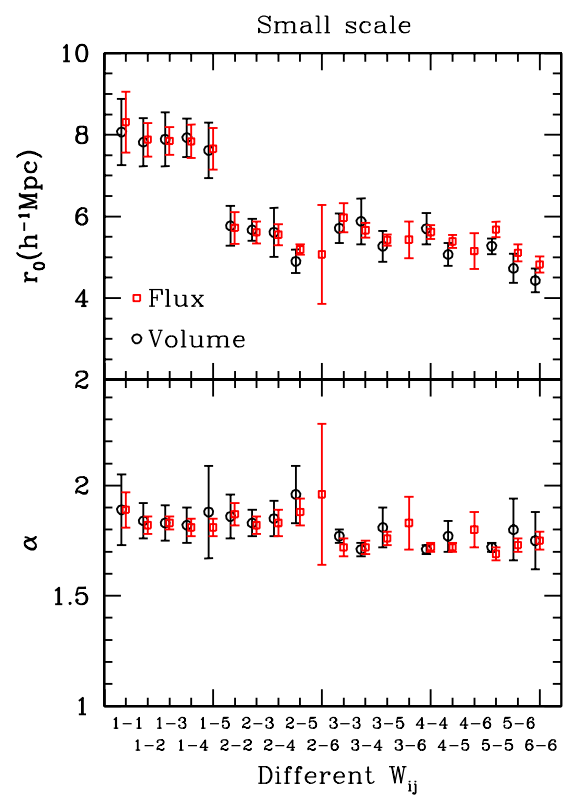


Fig. 4.— The same as Fig. 3 except that the results are obtained from the fitting to the correlation functions on small scales $(0.16 \ h^{-1}{\rm Mpc} \le r_p \le 0.98 \ h^{-1}{\rm Mpc})$.

4. DEPENDENCE ON GALAXY LUMINOSITY

We start our investigation by comparing the projected 2PCFs obtained using the volume-limited and flux-limited samples. When calculating the projected 2PCFs with the volume-limited samples, we use combinations of the set V1-V6 with the set Va-Vf for the reasons given in Section 3. Since the results are very similar for the volume-limited and the flux-limited samples, we show only the results for the flux-limited samples in Fig. 2, where we compare the projected 2PCFs based on random samples of type R1 with those based on random samples of type R2. As found by Li et al. (2006), the two types of random samples give almost identical results in most cases. The largest discrepancy is seen in the auto 2PCF of sample F5, This sample is significantly affected by the supercluter at redshift $z \sim 0.08$, and the points in sample R1 is not completely random due to the way it is constructed. Since overall the random samples of type R1 work quite well and since their construction does not require the luminosity function of galaxies, the results presented below will be based on this type of random samples. As one can see, brighter galaxies are on average more strongly clustered, an effect to be described in more detail in the following.

To quantify the observed 2PCFs, we fit to the projected 2PCFs according to Eq. (5) with the two free parameters r_0 and α . A larger value of r_0 implies a stronger clustering strength, while a larger α implies a steeper correlation function. In order to see how r_0 and α might change with scales, we fit the projected 2PCFs separately over two scale ranges, $0.98 \ h^{-1}{\rm Mpc} \le r_p \le 9.6 \ h^{-1}{\rm Mpc}$ and $0.16 \ h^{-1}{\rm Mpc} \le r_p \le 0.98 \ h^{-1}{\rm Mpc}$. The separation

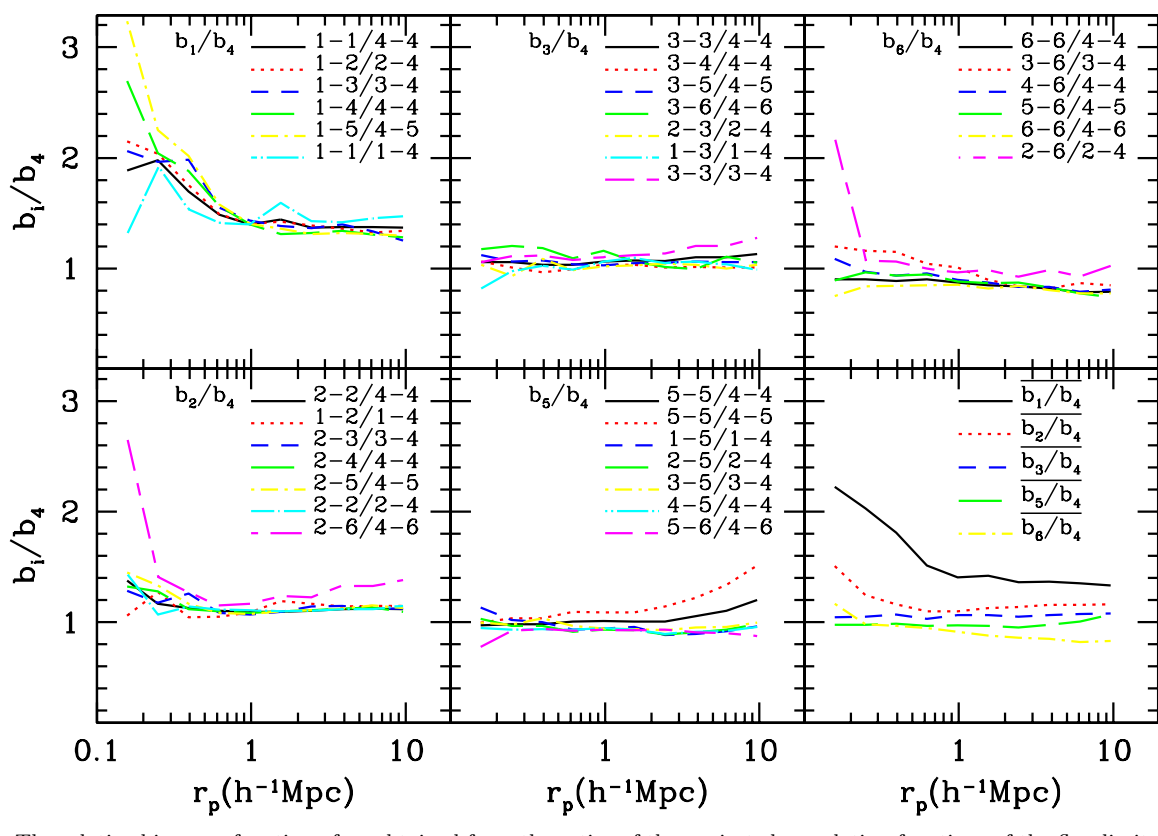


Fig. 5.— The relative bias as a function of r_p obtained from the ratios of the projected correlation functions of the flux-limited samples. In the lower-right panel, we show the mean relative bias parameters obtained by averaging the results shown in each of the five panels. In each panel, i-j means that the projected two-point correlation function is for samples Fi and Fj.

TABLE 5 The correlation lengths and slopes for flux-limited samples on large scales $(0.98\,h^{-1}{\rm Mpc} \le r_p \le 9.6\,h^{-1}{\rm Mpc})$

Sample	F1	F2	F3	F4	F5	F6
	α	α	α	α	α	α
	r_0	r_0	r_0	r_0	r_0	r_0
F1	1.81 ± 0.03					
	7.83 ± 0.61					
F2	1.80 ± 0.03	1.76 ± 0.03				
	6.88 ± 0.42	6.06 ± 0.22				
F3	1.84 ± 0.04	1.77 ± 0.04	1.73 ± 0.02			
	6.54 ± 0.33	5.82 ± 0.22	5.91 ± 0.14			
F4	1.80 ± 0.07	1.77 ± 0.05	1.79 ± 0.03	1.78 ± 0.03		
	6.36 ± 0.63	5.73 ± 0.27	5.47 ± 0.11	5.41 ± 0.13		
F5	1.81 ± 0.13	1.75 ± 0.07	1.77 ± 0.05	1.78 ± 0.03	1.64 ± 0.02	
	6.09 ± 0.88	5.46 ± 0.31	5.29 ± 0.17	5.17 ± 0.09	5.55 ± 0.15	
F6		1.76 ± 0.35	1.86 ± 0.20	1.83 ± 0.16	1.85 ± 0.09	1.88 ± 0.12
		5.59 ± 1.12	5.14 ± 0.48	4.96 ± 0.34	4.73 ± 0.14	4.49 ± 0.13
$\alpha = \overline{\alpha} = 1.79$	r_0	r_0	r_0	r_0	r_0	r_0
F1	7.80 ± 0.31					
F2	6.86 ± 0.21	6.09 ± 0.13				
F3	6.49 ± 0.19	5.83 ± 0.12	5.94 ± 0.14			
F4	6.34 ± 0.35	5.75 ± 0.18	5.48 ± 0.15	5.42 ± 0.14		
F5	6.07 ± 0.56	5.48 ± 0.29	5.31 ± 0.10	5.17 ± 0.09	5.65 ± 0.11	
F6		5.62 ± 0.46	5.08 ± 0.37	4.93 ± 0.21	4.68 ± 0.11	4.38 ± 0.12

TABLE 6 The correlation lengths and slopes for flux-limited samples on small scales $(0.16\,h^{-1}{\rm Mpc} \le r_p \le 0.98\,h^{-1}{\rm Mpc})$

Sample	F1	F2	F3	F4	F5	F6
	α	α	α	α	α	α
	r_0	r_0	r_0	r_0	r_0	r_0
F1	1.89 ± 0.08					
	8.31 ± 0.75					
F2	1.82 ± 0.04	1.87 ± 0.05				
	7.88 ± 0.41	5.72 ± 0.39				
F3	1.83 ± 0.03	1.82 ± 0.04	1.72 ± 0.04			
	7.85 ± 0.34	5.61 ± 0.27	5.97 ± 0.36			
F4	1.81 ± 0.04	1.83 ± 0.06	1.72 ± 0.03	1.72 ± 0.02		
	7.84 ± 0.41	5.55 ± 0.26	5.66 ± 0.18	5.62 ± 0.17		
F5	1.81 ± 0.04	1.88 ± 0.06	1.76 ± 0.03	1.72 ± 0.02	1.69 ± 0.03	
	7.66 ± 0.51	5.19 ± 0.13	5.42 ± 0.14	5.39 ± 0.16	5.68 ± 0.19	
F6		1.96 ± 0.32	1.83 ± 0.12	1.80 ± 0.08	1.73 ± 0.03	1.75 ± 0.04
		5.07 ± 1.21	5.43 ± 0.45	5.15 ± 0.44	5.11 ± 0.21	4.82 ± 0.20
$\alpha = \overline{\alpha} = 1.80$	r_0	r_0	r_0	r_0	r_0	r_0
F1	8.21 ± 0.42					
F2	7.17 ± 0.23	6.01 ± 0.19				
F3	6.93 ± 0.11	5.71 ± 0.19	5.61 ± 0.15			
F4	6.96 ± 0.13	5.69 ± 0.18	5.33 ± 0.06	5.29 ± 0.15		
F5	6.77 ± 0.16	5.50 ± 0.15	5.25 ± 0.17	5.10 ± 0.18	5.24 ± 0.14	
F6		5.69 ± 0.59	5.54 ± 0.09	5.13 ± 0.13	4.85 ± 0.17	4.64 ± 0.15

TABLE 7 THE CORRELATION LENGTHS AND SLOPES FOR FLUX-LIMITED SAMPLES OF RED GALAXIES ON LARGE SCALES $(0.98~h^{-1}{\rm Mpc} \le r_p \le 9.6~h^{-1}{\rm Mpc})$

Sample	$\mathrm{F1}_{\mathrm{red}}$	$\mathrm{F2}_{\mathrm{red}}$	$F3_{\rm red}$	$\mathrm{F4}_{\mathrm{red}}$	$\mathrm{F5}_{\mathrm{red}}$	$F6_{\rm red}$
	α	α	α	α	α	α
	r_0	r_0	r_0	r_0	r_0	r_0
$F1_{red}$	1.85 ± 0.04					
	8.73 ± 0.64					
$F2_{red}$	1.86 ± 0.05	1.82 ± 0.04				
	7.74 ± 0.48	6.95 ± 0.24				
$F3_{red}$	1.88 ± 0.06	1.84 ± 0.05	1.86 ± 0.03			
	7.38 ± 0.43	6.74 ± 0.24	6.51 ± 0.19			
$F4_{red}$	1.84 ± 0.10	1.83 ± 0.06	1.86 ± 0.04	1.86 ± 0.03		
	7.36 ± 0.72	6.73 ± 0.30	6.52 ± 0.18	6.52 ± 0.18		
$F5_{red}$	1.84 ± 0.15	1.85 ± 0.07	1.86 ± 0.05	1.89 ± 0.03	1.92 ± 0.02	
104	7.14 ± 1.00	6.56 ± 0.36	6.48 ± 0.24	6.39 ± 0.12	6.18 ± 0.11	
$F6_{red}$		1.94 ± 0.24	1.95 ± 0.19	1.94 ± 0.13	2.04 ± 0.07	2.07 ± 0.07
104		6.73 ± 1.11	6.67 ± 0.78	6.44 ± 0.56	6.24 ± 0.18	6.29 ± 0.18
$\alpha = \overline{\alpha} = 1.89$	r_0	r_0	r_0	r_0	r_0	r_0
$F1_{red}$	8.72 ± 0.48					
$F2_{red}$	7.74 ± 0.38	6.96 ± 0.25				
$F3_{red}$	7.38 ± 0.36	6.73 ± 0.25	6.51 ± 0.13			
$F4_{red}$	7.37 ± 0.39	6.73 ± 0.36	6.52 ± 0.21	6.51 ± 0.14		
$F5_{red}$	7.15 ± 0.32	6.56 ± 0.36	6.47 ± 0.23	6.39 ± 0.12	6.19 ± 0.09	
$F6_{red}$		6.74 ± 0.78	6.65 ± 0.19	6.44 ± 0.22	6.25 ± 0.29	6.27 ± 0.31

			Γ	[ABI	LE 8						
The correlation									RED	GALAXIES	ON
	SMALL SC	ALES	(0.16 h)	^{-1}M	$pc \le 1$	$r_p \le 0.98$	$8 h^{-1} \mathrm{Mpc}$	2)			

Sample	$F1_{red}$	$F2_{red}$	$F3_{red}$	$F4_{red}$	$F5_{red}$	$F6_{red}$
	α	α	α	α	α	α
	r_0	r_0	r_0	r_0	r_0	r_0
$F1_{red}$	1.90 ± 0.10					
	9.14 ± 0.90					
$F2_{red}$	1.85 ± 0.08	1.94 ± 0.06				
	9.00 ± 0.72	6.50 ± 0.21				
$F3_{red}$	1.86 ± 0.06	1.91 ± 0.04	1.85 ± 0.02			
	8.92 ± 0.54	6.48 ± 0.36	6.60 ± 0.29			
$F4_{red}$	1.86 ± 0.09	1.93 ± 0.06	1.82 ± 0.03	1.83 ± 0.02		
	8.93 ± 0.88	6.43 ± 0.37	6.77 ± 0.46	6.79 ± 0.28		
$F5_{red}$	1.85 ± 0.27	2.01 ± 0.22	1.84 ± 0.18	1.83 ± 0.12	1.83 ± 0.07	
	9.00 ± 1.02	6.09 ± 0.34	6.89 ± 0.36	6.84 ± 0.24	6.94 ± 0.16	
$F6_{red}$		1.87 ± 0.22	1.85 ± 0.28	1.94 ± 0.31	1.85 ± 0.18	1.92 ± 0.18
		8.87 ± 1.44	9.00 ± 0.56	6.69 ± 0.35	7.38 ± 0.24	7.35 ± 0.16
$\alpha = \overline{\alpha} = 1.88$	r_0	r_0	r_0	r_0	r_0	r_0
$F1_{red}$	9.03 ± 0.51					
$F2_{red}$	8.02 ± 0.43	6.86 ± 0.18				
$F3_{red}$	7.77 ± 0.33	6.65 ± 0.14	6.45 ± 0.31			
$F4_{red}$	7.92 ± 0.23	6.72 ± 0.16	6.50 ± 0.33	6.53 ± 0.26		
$F5_{red}$	7.83 ± 0.53	6.82 ± 0.18	6.67 ± 0.16	6.60 ± 0.24	6.64 ± 0.15	
$F6_{red}$		7.84 ± 0.79	7.09 ± 0.35	7.21 ± 0.37	7.67 ± 0.24	

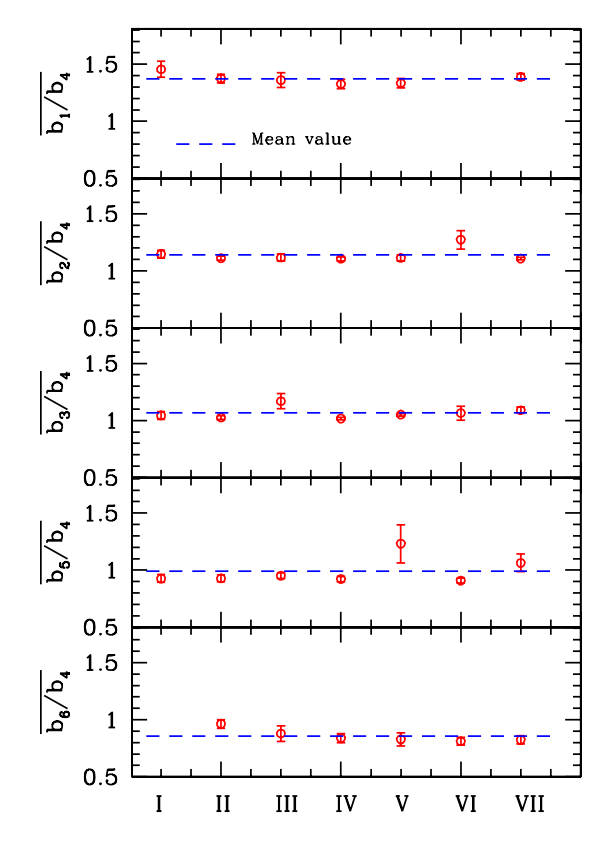


FIG. 6.— The relative bias parameters obtained from the correlation functions over $0.98\ h^{-1}{\rm Mpc}$ to $9.8\ h^{-1}{\rm Mpc}$ using seven different approaches (see the main text for details). The errorbars are based on the scatter of the data points in the range $0.98\ h^{-1}{\rm Mpc} < r_p \le 9.8\ h^{-1}{\rm Mpc}$. Panels from top to bottom correspond to the bias parameters for Fi (i=1,2,3,5,6), normalized by that of F4. The horizontal axis labels the different approaches that are used to determine the bias parameter for each subsample. One data point is missing in the first and fifth panels, because the redshift overlap between F1 and F6 is too small to measure the cross-correlation function reliably.

between large and small scales is made at $r_p \sim 1 h^{-1} {\rm Mpc}$, because the correlation function on smaller scales is expected to be dominated by the one-halo term, while that on larger scales by the two-halo term, as shown in Yang et al. (2005). We use two methods to obtain r_0 and α from the data. In the first method, we obtain r_0 and α directly from the fit to the projected 2PCFs. In the second one, we first obtain an average value of α , $\overline{\alpha}$, from all the correlation functions and then fit the projected 2PCF to get r_0 keeping $\alpha = \overline{\alpha}$. The fitting parameters so obtained are listed in Tables 3, 4, 5 and 6, separately for volume-limited and flux-limited samples, and for large and small scales.

Fig. 3 compares the values of r_0 and α on large scales $(0.98 \ h^{-1}{\rm Mpc} \le r_p \le 9.6 \ h^{-1}{\rm Mpc})$ obtained from the volume-limited samples with those obtained from the corresponding flux-limited samples. Overall, the results for these two kinds of samples are similar. The only exception is $W_{5,5}$, where the values of r_0 and α for the volume-limited and flux-limited samples are significantly different, largely because the presence of the supercluster at $z \sim 0.08$ that makes the correlation properties quite sensitive to how the sample is exactly formed. There is a clear trend in the correlation length r_0 that brighter galaxies have larger r_0 . The cross-correlations between bright and faint galaxies are also stronger than the auto correlations of faint galaxies. On the other hand the slope of the correlation function does not show any strong trend with luminosity, and the mean value of and scatter in α are 1.82 ± 0.04 for the volume-limited samples and 1.79 ± 0.05 for the flux-limited samples. The correlation lengths obtained by fixing α at these mean values are also listed in Tables 3, 4, 5 and 6 for comparison.

In order to investigate how the clustering strengths change on small scales, we fit the projected 2PCFs with power laws in the range 0.16 $h^{-1}{\rm Mpc} \le r_p \le 0.98 \ h^{-1}{\rm Mpc}$, and the results are shown in Fig. 4 and listed in Tables 4 and 6. A comparison to the results

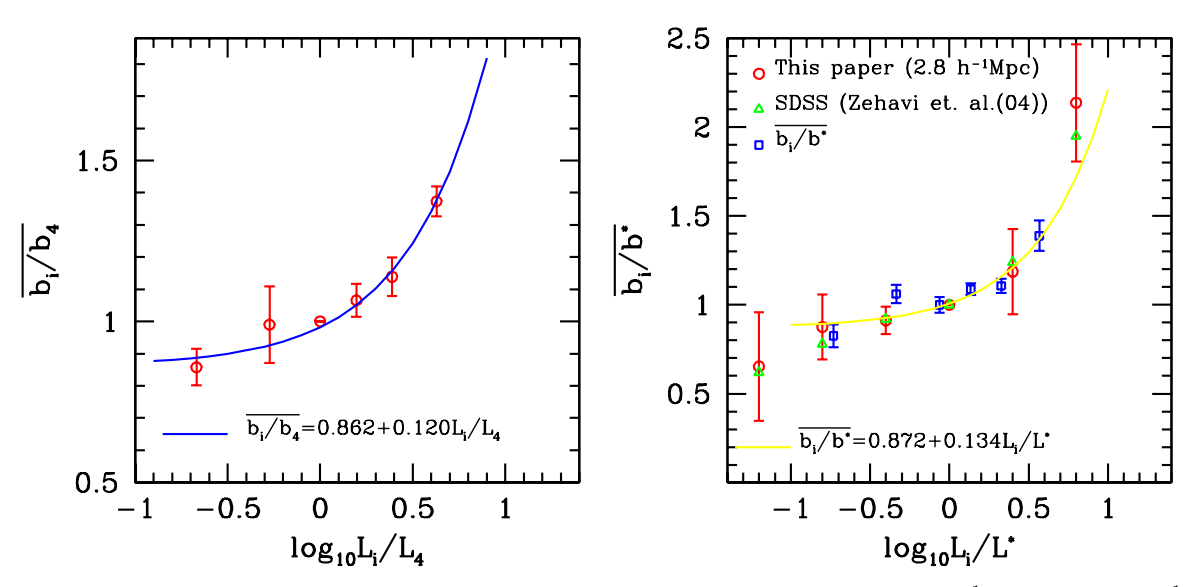


FIG. 7.— Left panel: The average relative bias parameter, obtained using the correlation data in $0.98\,h^{-1}{\rm Mpc} < r_p \le 9.8\,h^{-1}{\rm Mpc}$ as a function of galaxy luminosity. The results are obtained using the flux-limited samples, and both the bias parameter and the luminosity are normalized by the values for F4. For a given liminosity, the mean and errorbar are based on the different measurements shown in Fig 6. The solid curve shows the relation, $\overline{b_i/b_4} = 0.862 + 0.120L_i/L_4$, obtained by fitting the data. Right panel: In this panel, we compare our results with those obtained by Zehavi et al. (2005). Here the bias parameters and the luminosities are normalized by the values for L^* galaxies. In Zehavi et al., the relative bias parameters are measured using the auto-correlation functions at $r_p = 2.8\,h^{-1}{\rm Mpc}$ for six volume-limited samples with luminosities in (-23.0, -22.0), (-22.0, -21.0), (-21.0, -20.0), (-20.0, -19.0), (-19.0, -18.0), (-18.0, -17.0), and their results are shown by triangles. Our results for a similar analysis are shown as open circles and match very well their results. The open squares show the same results as shown in the left panel, except that the normalizations are different. The curve is a fit to the results represented by the open squares.

shown in Fig. 3 shows that the clustering strengths for the samples that involve the brightest galaxies are enhanced on small scales; in particular the cross correlation between the brightest and faintest galaxies is much stronger on small scales. For faint galaxies, the clustering strengths on small scales are similar to those based on the power laws obtained on large scales. This suggests that there is a significant population of faint galaxies that are distributed around the brightest galaxies and the number drops rapidly with the increase of the distance to the brightest galaxies. As we will see below, it is likely that this population is dominated by faint red galaxies in clusters and groups. On average, faint galaxies are more uniformly distributed than bright galaxies, presumably because the majority of the faint galaxies are in the field.

Having investigated the clustering strengths for galaxies of different luminosities, we now study the bias factor in the distribution of galaxies as a function of galaxy luminosity. Since we do not know the two-point correlation function of the cosmic density field, we can only study the bias factor in a relative sense. To do this, we choose F4 as our fiducial sample, because it has a good overlap in volume with both the faint and bright samples. Since each sample is used in a number of projected 2PCFs, we can estimate the relative bias for each sample in a number of ways. With F4 as the reference sample, the bias factor for the *i*th sample can be estimated from one of the following definitions:

$$\frac{b_i}{b_4} = \frac{W_{i,j}}{W_{j,4}} (j = 1, 2, 3, 4, 5, 6),$$

$$\frac{b_i}{b_4} = \sqrt{\frac{W_{i,i}}{W_{4,4}}},$$
(6)

where i=1,2,3,5,6. Thus, each relative bias can be estimated using seven different approaches. In what follows, these seven approaches will be referred as approaches I, II, ..., VI, corresponding to $j=1,2,\dots,6$, respectively, and approach VII, corresponding to the definition in the second line of equation (6). Note that in general the relative bias factors, b_i/b_4 , obtained from different approaches are not expected to be the same. As we will discuss in Section 6, these relative bias factors are expected to be the same only under the assumption that the bias for galaxies of different luminosities is linear and that the stochastic component in the bias relations between different galaxies is small.

The first 5 panels in Fig. 5 show the relative bias factor as a function of r_p for the five samples, Fi (i=1,2,3,5,6), and the 7 different lines within each panel show the results obtained using the 7 different approaches described above. For most cases, the bias function is almost independent of r_p at $r_p > 1 \, h^{-1}{\rm Mpc}$, indicating that nonlinearity in the relative bias is small on these scales. The bias factors obtained using the 7 different approaches agree quite well with each other, and their averages are shown in the last panel. we see clearly that brighter galaxies have higher relative biases.

To quantify the relative bias as a function of luminosity, we estimate a mean relative bias factor for each case by averaging the bias function over $1h^{-1}\mathrm{Mpc}$ - $10h^{-1}\mathrm{Mpc}$. The results are shown in Fig. 6 for different luminosity samples using the 7 approaches. Note that there is one data point missing in the first and fifth panels, because the overlap between samples F1 and F6 is too small to have a reliable measurement of $W_{1,6}$. The dashed line in each panel is the average value of the relative bias obtained from the seven different approaches. As one can see, the relative bias factors obtained with different ap-

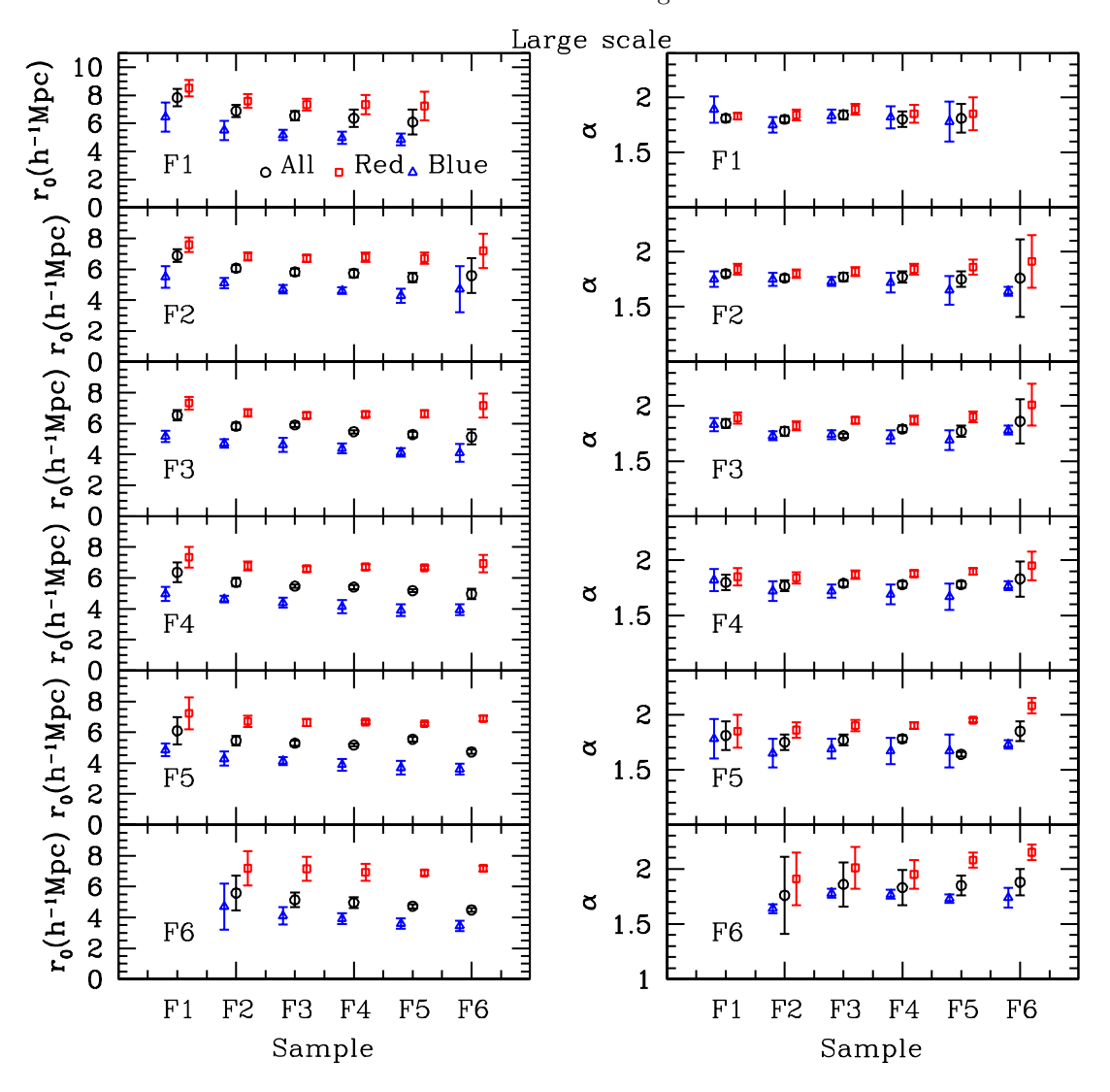


FIG. 8.— Here we compare the correlation lengths (r_0) and slopes (α) of all (circles), red (squares) and blue (triangles) galaxies using flux-limited samples (F1 – F6 for all galaxies; F1_{red} – F6_{red} for red galaxies, and F1_{blue} – F6_{blue} for blue galaxies). Here the results are based on correlation functions on large scales, $0.98 \, h^{-1}{\rm Mpc} \le r_p \le 9.6 \, h^{-1}{\rm Mpc}$. To avoid confusion, data points for rad and blue galaxies are shifted slightly horizontally.

proaches are consistent with each other. We estimate the mean absolute magnitude of galaxies in each sample as

$$\overline{M_i} = \frac{1}{N_i} \sum_{n=1}^{N_i} M_n \,, \tag{7}$$

where M_n is the absolute magnitude of the nth galaxy in sample Fi, and N_i is the galaxy number in this sample. Note that this definition is not physical but is chosen to characterize the luminosities of galaxies in a sample. The average absolute magnitudes for sample F1–F6 thus obtained are -21.83, -21.23, -20.75, -20.26, -19.58, and -18.59, respectively. These magnitudes are then converted into luminosities to represent the characteristic luminosities of the samples in question. The left panel of Fig. 7 shows the average relative bias factor versus L_i/L_4 as open circles, with errorbars representing the scatter among the seven different approaches. There is a clear trend that the relative bias increases with galaxy

luminosity. The solid curve is a linear fit to the data: $\overline{b_i/b_4} = 0.862 + 0.120L_i/L_4$.

The luminosity dependence of galaxy bias in the SDSS has been investigated by Zehavi et al. (2005) using the amplitudes of the auto correlation functions at a fixed projected radius $r_p = 2.7 \ h^{-1}{\rm Mpc}$ obtained from six volume-limited samples with M_r in (-23, -22), (-22, -21), (-21, -20), (-20, -19), (-19, -18), (-18, -17). The bias factors were normalized relative to L^* galaxies defined to be the ones with M_r in (-21, -20). To compare our results with theirs, we show in the right panel of Fig. 7 the relative bias factors obtained by Zehavi et al. as triangles together with our results (open circles) that are obtained from the autocorrelation amplitudes at a fixed, but a slightly different, projected radius $r_p = 2.8 h^{-1} \text{Mpc}$. Note that our results are in excellent agreement with the results obtained by Zehavi et al. (2005). For the relative bias - luminosity

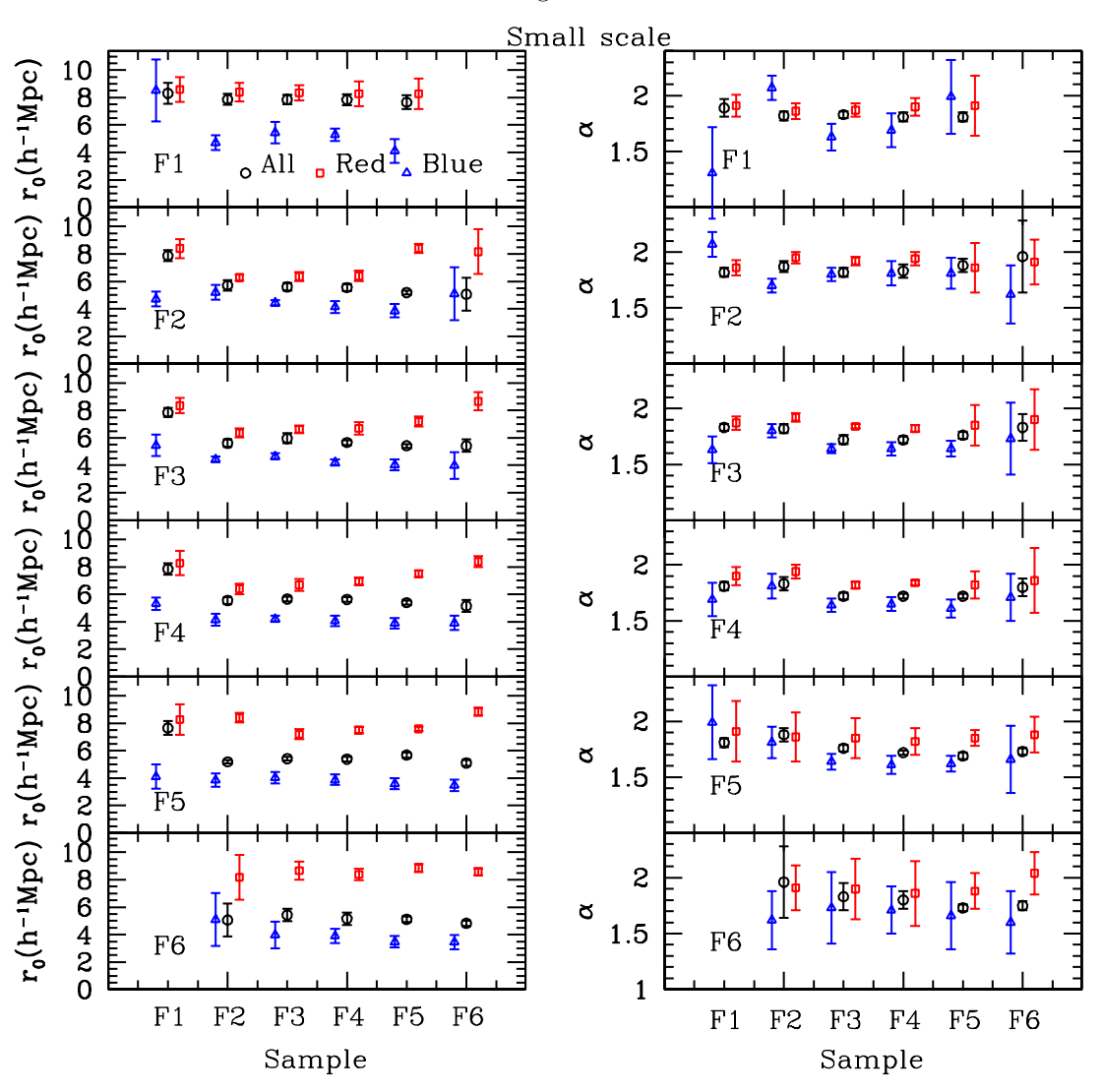


Fig. 9.— The same as Fig. 8, except that the results are based on the correlation functions on small scales, $0.16 \ h^{-1}{\rm Mpc} \le r_p \le 0.98 \ h^{-1}{\rm Mpc}$.

relation shown in the left panel of Fig. 7, we can convert it into a relation with L/L^* . The characteritic luminosity for sample F* is -20.45, very close to L^* . Using the projected 2PCF for F*, $W_{\star,\star}$, we can write

$$\overline{b_i/b^*} = \overline{b_i/b_4} \sqrt{\frac{W_{4,4}}{W_{*,*}}},$$
(8)

where $W_{4,4}$ and $W_{*,*}$ are the projected auto 2PCFs of samples F4 and F*, respectively. The resulting $\overline{b_i/b^*}$ - L/L_{\star} relation is shown by the open squares in the right panel of Fig. 7. Fitted with a linear model, this relation can be desribed as $b_i/b^* = 0.872 + 0.134L_i/L^*$. As one can see, our results based on the cross-correlation match well those of Zehavi et al. (2005). We will come back in Section 6 about the implications of this agreement.

5. DEPENDENCE ON GALAXY COLOR

In order to study how galaxy clustering depends on both galaxy luminosity and color, we have subdivided

each flux-limited sample, Fi, into a red and a blue subsample according to the criteria decribed in equation (1). We remind that these subsamples are referred to as Fired and Fiblue. We have carried out the same analysese as described in Section 4 for these color samples. Figs. 8 shows the correlation lengths r_0 and slopes α obtained by fitting the correlation functions in the range $0.98 h^{-1} \text{Mpc} \le r_p \le 9.6 h^{-1} \text{Mpc}$; the corresponding results for small scales, $0.16 h^{-1} \text{Mpc} \le r_p \le 0.98 h^{-1} \text{Mpc}$, are shown in Figs. 9. In both figures, we also include the results for the total samples (i.e. without color separation) for comparison. Again, the errorbars are obtained from the scatter among the three regions in the SDSS observations. To make the results accessible to others, we list all the values of r_0 and α in Tables 7 (red galaxies; large scales), 8 (red galaxies; small scales), 9 (blue galaxies; large scales), and 10 (blue galaxies; small scales). In all these tables, we also include the best fit values for r_0 by fixing $\alpha = \overline{\alpha}$.

As one can see clearly from the left panels in Fig. 8,

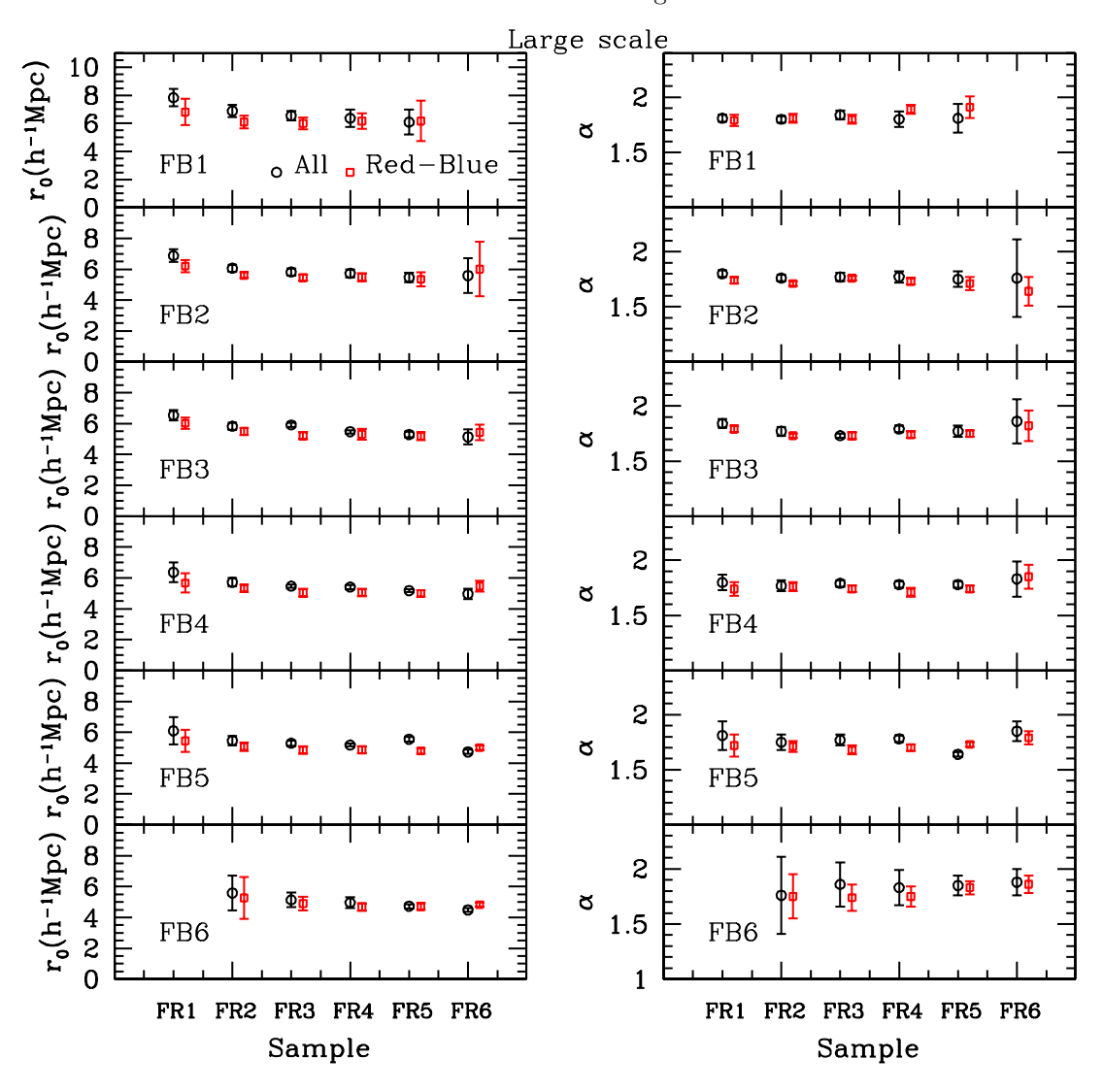


Fig. 10.— The correlation lengths (r_0) and slopes (α) of the cross-correlation functions between red and blue galaxies (squares) on large scales, 0.98 $h^{-1}{\rm Mpc} \le r_p \le 9.6 \ h^{-1}{\rm Mpc}$. Panels from top to bottom correspond to flux limited samples for blue galaxies FBi $\equiv {\rm Fi}_{\rm blue}$ (i=1,2...,6). The red samples used in the cross-corelations are labeled on the horizontal axis FRi $\equiv {\rm Fi}_{\rm red}$ (i=1,2...,6). For comparison, results for all galaxies in the corresponding flux-limited samples are plotted as open circles.

on large scales red galaxies in general have larger r_0 than all galaxies and blue galaxies in the same luminosity bin. Thus, the color dependence is not particular only to some specific luminosities. Note also that the luminosity dependence of r_0 is seen in all, red and blue samples, although the dependence is stronger for blue galaxies, as to be quantified in the following. Overall, the correlation slope, α (showin in the right panel of Fig. 8) is larger for red galaxies, and the dependence is stronger for the cases where at least one of the two samples in cross-correlation is faint.

As shown in Fig. 9, the correlation lengths r_0 obtained from the projected 2PCFs on small scales have properties similar to those on large scales, in that red galaxies have a larger correlation length. But the trend is quite different in detail. Firstly, the difference between the correlation lengths obtained from the cross correlations of the brightest red sample (F1_{red}) with other red samples are

significantly larger here than that shown in Fig. 9. Since the brightest red galaxies are located predominately in clusters and rich groups, this suggests that many of the the faint red galaxies are also in clusters and groups. Secondly, for F3_{red} through F5_{red}, their cross-correlation with the faintest red galaxies has an amplitude that is significantly larger than their cross-correlation with brighter (except the brightest) red galaxies. This indicates that many red galaxies of intermediate luminosities may possess halos of red satellite galaxies that are more than 1 magnitudes fainter. Finally, on small scales, the luminosity-dependence r_0 for blue galaxies appears to be weaker.

It is also interesting to look at the cross correlation between red and blue galaxies. In Figs. 10 and 11, we compare the values of r_0 and α for such cross correlations on large and small scales with those for all galaxies. These values are also listed in Tables 11 and 12. As one can

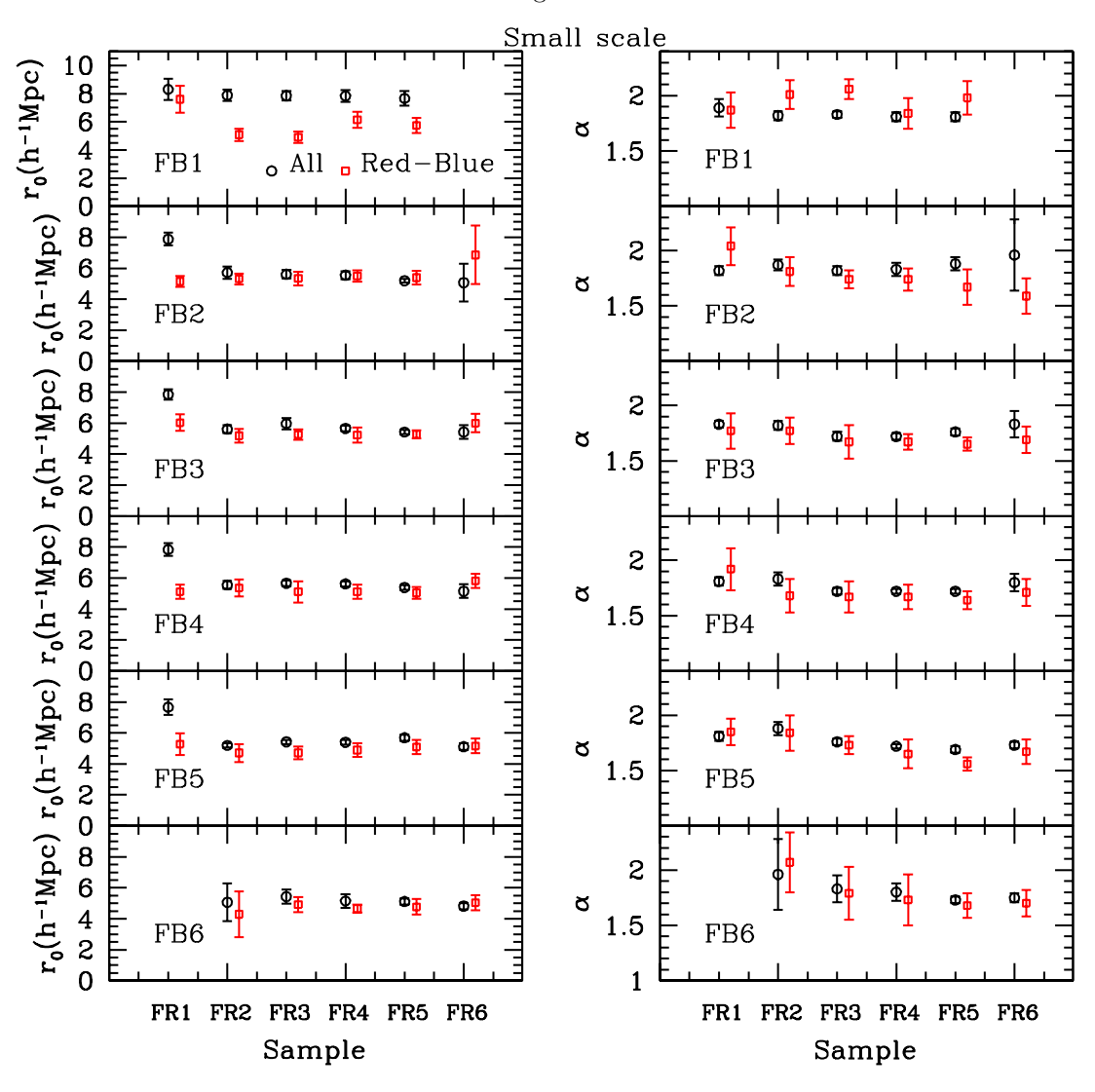


Fig. 11.— The same as Fig. 10, but here results are based on correlation functions on small scales, $0.16\,h^{-1}{\rm Mpc} \le r_p \le 0.98\,h^{-1}{\rm Mpc}$.

see, on large scales $(0.98 \ h^{-1}{\rm Mpc} \le r_p \le 9.6 \ h^{-1}{\rm Mpc})$ (Fig. 10), the values of r_0 and α for the red/blue cross-correlation functions are quite similar to those for all galaxies. However, there is a marked difference on small scales $(0.16 h^{-1}{\rm Mpc} \le r_p \le 0.98 h^{-1}{\rm Mpc})$ (Fig. 11). Here the cross correlation amplitudes between the brightest red galaxies (F1_{red}) and blue galaxies are significantly lower than those for all galaxies. Since many of the brightest red galaxies are the brightest central galaxies in clusters and groups, this result suggests the satellite galaxies of these galaxies are preferentially red, in qualitative agreement with the findings by Weinmann et al. (2006).

In order to quantify how galaxies of different colors and luminosities are biased with respect to each other on large scales, we measure the relative bias factors for red and blue galaxies based on the ratios of the corresponding projected 2PCFs, as we did in Section 4 for the luminosity samples. Note that, in addition to the red-red and blue-blue cross-correlation functions among

the 6 luminosity bins, one can also use the red-blue cross-correlation functions to obtain the relative bias. These are

$$\frac{b_i}{b_4} = \frac{W_{Ri,Bj}}{W_{R4,Bj}} \tag{9}$$

for red galaxies, and

$$\frac{b_i}{b_4} = \frac{W_{Bi,Rj}}{W_{B4,Rj}} \tag{10}$$

for blue galaxies, where i=1,2,3,5,6 and j=1,2,3,4,5,6, and Bi and Ri denotes Fi_{blue} and Fi_{red}, respectively. Together with the previous seven approaches, we have now in total 13 approaches to measure the relative bias b_i/b_4 for each red or blue subsamples. Figs. 12 and 13 show the large-scale relative bias factors obtained with the 13 approaches for red and blue galaxies, respectively. Some points are missing again because the overlaps of the samples in question are too small. The dashed line in each panel is the average value of the relative bias. As one can see, most of the approaches give consistent

TABLE 9 THE CORRELATION LENGTH AND SLOPE FOR FLUX-LIMITED SAMPLES OF BLUE GALAXIES ON LARGE SCALES (0.98 $h^{-1}{\rm Mpc} \le r_p \le 9.6~h^{-1}{\rm Mpc})$

Sample	$F1_{blue}$	$F2_{blue}$	$F3_{blue}$	$F4_{blue}$	$F5_{blue}$	$F6_{blue}$
	α	α	α	α	α	α
	r_0	r_0	r_0	r_0	r_0	r_0
$F1_{blue}$	1.84 ± 0.06					
	6.70 ± 0.96					
$F2_{blue}$	1.76 ± 0.06	1.72 ± 0.06				
	5.86 ± 0.65	5.08 ± 0.34				
$F3_{blue}$	1.82 ± 0.06	1.71 ± 0.05	1.74 ± 0.04			
	5.62 ± 0.32	4.70 ± 0.29	4.64 ± 0.46			
$F4_{blue}$	1.79 ± 0.10	1.73 ± 0.09	1.74 ± 0.06	1.69 ± 0.09		
	5.24 ± 0.42	4.59 ± 0.19	4.34 ± 0.32	4.07 ± 0.43		
$F5_{blue}$	1.71 ± 0.18	1.66 ± 0.13	1.69 ± 0.09	1.67 ± 0.12	1.65 ± 0.15	
	4.89 ± 0.36	4.31 ± 0.49	4.02 ± 0.27	3.78 ± 0.38	3.48 ± 0.44	
$F6_{blue}$		1.66 ± 0.04	1.78 ± 0.04	1.77 ± 0.04	1.70 ± 0.04	1.77 ± 0.09
		4.77 ± 1.46	4.02 ± 0.58	3.76 ± 0.38	3.35 ± 0.39	3.19 ± 0.31
$\alpha = \overline{\alpha} = 1.73$	r_0	r_0	r_0	r_0	r_0	r_0
$F1_{blue}$	6.48 ± 0.58					
$F2_{blue}$	5.80 ± 0.23	5.11 ± 0.26				
$F3_{blue}$	5.43 ± 0.17	4.78 ± 0.21	4.61 ± 0.24			
$F4_{blue}$	5.10 ± 0.21	4.60 ± 0.31	4.33 ± 0.24	4.13 ± 0.23		
$F5_{blue}$	4.91 ± 0.36	4.41 ± 0.29	4.09 ± 0.21	3.87 ± 0.18	3.60 ± 0.13	
$F6_{blue}$		4.92 ± 0.69	3.92 ± 0.23	3.71 ± 0.37	3.39 ± 0.19	3.14 ± 0.13

TABLE 10 The correlation length and slope for flux-limited samples of blue galaxies on small scales (0.16 $h^{-1}{\rm Mpc} \le r_p \le 0.98\,h^{-1}{\rm Mpc})$

Sample	$F1_{blue}$	$F2_{blue}$	$F3_{blue}$	$F4_{blue}$	$F5_{blue}$	$F6_{blue}$
	α	α	α	α	α	α
	r_0	r_0	r_0	r_0	r_0	r_0
$F1_{blue}$	1.93 ± 0.10					
	6.26 ± 0.85					
$F2_{blue}$	1.93 ± 0.09	1.83 ± 0.07				
	5.37 ± 0.52	4.86 ± 0.58				
$F3_{blue}$	1.69 ± 0.12	1.80 ± 0.06	1.65 ± 0.04			
	5.71 ± 0.72	4.45 ± 0.20	4.53 ± 0.22			
$F4_{blue}$	1.87 ± 0.15	1.78 ± 0.11	1.65 ± 0.06	1.69 ± 0.06		
0000	5.03 ± 0.45	4.31 ± 0.44	4.20 ± 0.24	3.85 ± 0.39		
$F5_{blue}$	2.05 ± 0.33	1.76 ± 0.14	1.63 ± 0.07	1.60 ± 0.08	1.65 ± 0.07	
5740	4.00 ± 0.88	4.03 ± 0.49	3.92 ± 0.41	3.64 ± 0.38	3.33 ± 0.39	
$F6_{blue}$		1.57 ± 0.26	1.67 ± 0.32	1.62 ± 0.21	1.67 ± 0.30	1.60 ± 0.28
		5.31 ± 1.92	4.02 ± 0.97	3.84 ± 0.52	3.18 ± 0.42	3.15 ± 0.51
$\alpha = \overline{\alpha} = 1.73$	r_0	r_0	r_0	r_0	r_0	r_0
$F1_{blue}$	7.28 ± 0.46					
$F2_{blue}$	6.11 ± 0.24	5.15 ± 0.23				
$F3_{blue}$	5.70 ± 0.36	4.65 ± 0.26	4.36 ± 0.28			
$F4_{blue}$	5.47 ± 0.32	4.43 ± 0.20	4.01 ± 0.16	3.81 ± 0.22		
$F5_{blue}$	4.78 ± 0.34	4.09 ± 0.26	3.75 ± 0.24	3.46 ± 0.24	3.29 ± 0.16	
$F6_{blue}$		5.00 ± 0.65	3.97 ± 0.22	3.64 ± 0.16	3.17 ± 0.17	2.96 ± 0.13

results. The exceptions are the results based on the cross correlations $F2_{\rm red}$ - $F6_{\rm blue}$, $F2_{\rm blue}$ - $F6_{\rm blue}$ and $F2_{\rm blue}$ - $F6_{\rm red}$. The volume overlap in each of these three sample pairs is quite small, and the corresponding results are quite uncertain.

In the left panels of Fig. 14 (upper panel for red galaxies and lower panel for blue galaxies), we show the average relative bias $(\overline{b_i/b_4})$ obtained from the 13 approaches) versus luminosity L_i/L_4 , where L_i for each sample is estimated in the same way as described in Section 4. Fitting to the data with a linear model gives $\overline{b_i/b_4} = 0.953 + 0.057L_i/L_4$ for red galaxies, and $\overline{b_i/b_4} = 0.860 + 0.132L_i/L_4$ for blue galaxies. As one can

see, the luminosity-dependence is much stronger for blue galaxies than for red galaxies. For red galaxies, significant luminosity-dependence is seen only at the brightest end, and there is indication that the bias factor becomes larger for the faintest sample.

In order to put the bias factors for different galaxies in the same absolute scale, we normalize all bias factors relative to that for all the galaxies (blue and red) in the F^* sample, i.e. we define

$$\overline{b_i/b^*} = \overline{b_i/b_4} \sqrt{\frac{W_{R4,R4}}{W^{*,*}}} \tag{11}$$

TABLE 11 The correlation length and slope between red and blue galaxies on large scales $(0.98\,h^{-1}{\rm Mpc} \le r_p \le 9.6\,h^{-1}{\rm Mpc})$

Sample	$F1_{red}$	$F2_{red}$	$F3_{red}$	$F4_{red}$	$F5_{red}$	$F6_{red}$
	α	α	α	α	α	α
	r_0	r_0	r_0	r_0	r_0	r_0
$F1_{blue}$	1.80 ± 0.03	1.85 ± 0.03	1.87 ± 0.03	1.88 ± 0.04	1.90 ± 0.07	
	7.41 ± 0.81	6.76 ± 0.36	6.59 ± 0.35	6.61 ± 0.52	6.43 ± 1.24	
$F2_{blue}$	1.74 ± 0.03	1.73 ± 0.02	1.76 ± 0.02	1.74 ± 0.03	1.71 ± 0.06	1.64 ± 0.13
	6.33 ± 0.41	5.76 ± 0.19	5.57 ± 0.19	5.51 ± 0.27	5.35 ± 0.45	5.85 ± 1.76
$F3_{blue}$	1.78 ± 0.03	1.75 ± 0.02	1.75 ± 0.03	1.73 ± 0.03	1.75 ± 0.03	1.83 ± 0.14
	6.03 ± 0.33	5.54 ± 0.21	5.24 ± 0.21	5.23 ± 0.35	5.06 ± 0.26	5.09 ± 0.51
$F4_{blue}$	1.72 ± 0.06	1.75 ± 0.04	1.75 ± 0.03	1.69 ± 0.04	1.73 ± 0.03	1.84 ± 0.11
	5.67 ± 0.64	5.29 ± 0.24	5.00 ± 0.27	4.92 ± 0.25	4.78 ± 0.21	4.91 ± 0.36
$F5_{blue}$	1.68 ± 0.10	1.70 ± 0.05	1.66 ± 0.04	1.66 ± 0.03	1.70 ± 0.02	1.76 ± 0.06
	5.20 ± 0.76	4.92 ± 0.27	4.66 ± 0.24	4.58 ± 0.22	4.45 ± 0.18	4.49 ± 0.14
$F6_{blue}$		1.73 ± 0.20	1.72 ± 0.13	1.73 ± 0.09	1.76 ± 0.06	1.79 ± 0.08
		5.12 ± 1.21	4.63 ± 0.45	4.42 ± 0.22	4.26 ± 0.23	4.21 ± 0.14
$\alpha = \overline{\alpha} = 1.75$	r_0	r_0	r_0	r_0	r_0	r_0
$F1_{blue}$	7.34 ± 0.42	6.63 ± 0.14	6.45 ± 0.15	6.45 ± 0.12	6.30 ± 0.18	
$F2_{blue}$	6.36 ± 0.12	5.80 ± 0.10	5.55 ± 0.18	5.53 ± 0.17	5.41 ± 0.13	6.02 ± 0.56
$F3_{blue}$	5.99 ± 0.11	5.55 ± 0.07	5.25 ± 0.13	5.26 ± 0.14	5.08 ± 0.13	4.98 ± 0.12
$F4_{blue}$	5.73 ± 0.17	5.30 ± 0.21	5.01 ± 0.19	4.98 ± 0.16	4.82 ± 0.18	4.78 ± 0.15
$F5_{blue}$	5.34 ± 0.11	5.00 ± 0.11	4.80 ± 0.17	4.70 ± 0.13	4.52 ± 0.09	4.49 ± 0.16
$F6_{blue}$		5.17 ± 0.69	4.71 ± 0.28	4.44 ± 0.32	4.25 ± 0.19	4.16 ± 0.17

TABLE 12 The correlation length and slope between red and blue galaxies on small scales $(0.16~h^{-1}{\rm Mpc} \le r_p \le 0.98~h^{-1}{\rm Mpc})$

Sample	$F1_{red}$	$F2_{red}$	$F3_{red}$	$F4_{red}$	$F5_{red}$	$F6_{red}$
	α	α	α	α	α	α
	r_0	r_0	r_0	r_0	r_0	r_0
$F1_{blue}$	1.85 ± 0.15	1.84 ± 0.09	1.83 ± 0.09	1.84 ± 0.12	1.84 ± 0.13	
	7.84 ± 0.86	7.80 ± 0.37	7.88 ± 0.35	7.86 ± 0.52	7.88 ± 0.51	
$F2_{blue}$	1.95 ± 0.17	1.80 ± 0.10	1.76 ± 0.08	1.74 ± 0.10	1.72 ± 0.16	1.62 ± 0.15
	5.50 ± 0.32	5.49 ± 0.37	5.45 ± 0.44	5.61 ± 0.35	5.35 ± 0.46	6.75 ± 1.93
$F3_{blue}$	1.79 ± 0.16	1.75 ± 0.12	1.59 ± 0.55	1.67 ± 0.07	1.61 ± 0.06	1.68 ± 0.12
	6.06 ± 0.52	5.25 ± 0.44	5.47 ± 0.35	5.06 ± 0.48	5.34 ± 0.27	5.45 ± 0.57
$F4_{blue}$	1.90 ± 0.19	1.67 ± 0.15	1.62 ± 0.14	1.62 ± 0.11	1.58 ± 0.08	1.70 ± 0.12
orac	5.08 ± 0.45	5.24 ± 0.56	5.17 ± 0.68	5.07 ± 0.46	5.03 ± 0.37	5.21 ± 0.45
$F5_{blue}$	1.81 ± 0.12	1.74 ± 0.16	1.65 ± 0.08	1.64 ± 0.13	1.54 ± 0.06	1.65 ± 0.11
orac	5.13 ± 0.71	4.77 ± 0.58	4.68 ± 0.42	4.55 ± 0.45	4.62 ± 0.46	4.54 ± 0.48
$F6_{blue}$		1.88 ± 0.29	1.76 ± 0.26	1.65 ± 0.24	1.63 ± 0.11	1.59 ± 0.12
- 01 4 C		4.66 ± 1.37	4.65 ± 0.55	4.36 ± 0.29	4.27 ± 0.55	4.36 ± 0.55
$\alpha = \overline{\alpha} = 1.71$	r_0	r_0	r_0	r_0	r_0	r_0
$F1_{blue}$	8.16 ± 0.49	7.41 ± 0.21	7.40 ± 0.27	8.02 ± 0.30	7.97 ± 0.29	
$F2_{blue}$	6.51 ± 0.31	5.83 ± 0.16	5.63 ± 0.13	5.73 ± 0.16	5.39 ± 0.21	6.27 ± 0.55
$F3_{blue}$	6.37 ± 0.37	5.38 ± 0.13	5.06 ± 0.12	5.04 ± 0.15	4.98 ± 0.15	5.45 ± 0.26
$F4_{blue}$	5.74 ± 0.41	5.23 ± 0.35	4.88 ± 0.34	4.77 ± 0.38	4.64 ± 0.35	5.15 ± 0.28
$F5_{blue}^{blue}$	5.45 ± 0.27	4.87 ± 0.33	4.48 ± 0.25	4.31 ± 0.34	4.16 ± 0.19	4.38 ± 0.27
$F6_{blue}$		5.14 ± 0.75	4.76 ± 0.24	4.24 ± 0.19	4.06 ± 0.28	4.05 ± 0.24

for red galaxies, and

$$\overline{b_i/b^*} = \overline{b_i/b_4} \sqrt{\frac{W_{B4,B4}}{W^{*,*}}} \tag{12}$$

for blue galaxies. Here $W_{R4,R4}$, $W_{B4,B4}$ and $W^{*,*}$ are the projected auto 2PCFs for $F4_{red}$, $F4_{blue}$ and F*, respectively. The values of $\overline{b_i/b^*}$ versus L/L^* are shown in the right panels of Fig. 14 (upper panel for red galaxies and lower panel for blue galaxies). Normalized in this way, the bias factors for red galaxies are all larger than 1, while those for blue galaxies smaller than 1, for the luminosity range probed here. Fitting the luminosity dependence with a linear model, we get $\overline{b_i/b^*}=1.352+0.096L_i/L^*$

for red galaxies, and $\overline{b_i/b^*}=0.560+0.101L_i/L^*$ for blue galaxies. Note that the constant component in the relation is much larger for red galaxies than for blue galaxies, although the linear terms are similar, implying again that the luminosity-dependence of the bias is weaker for red galaxies. These results are in good agreement with those obtained in Zehavi et al. (2005) based on autocorrelation functions.

6. NON-LINEAR AND STOCHASTIC BIAS

In the last two sections we have analyzed the autoand cross-correlation functions for galaxies of different luminosities and colors. We have seen that on scales

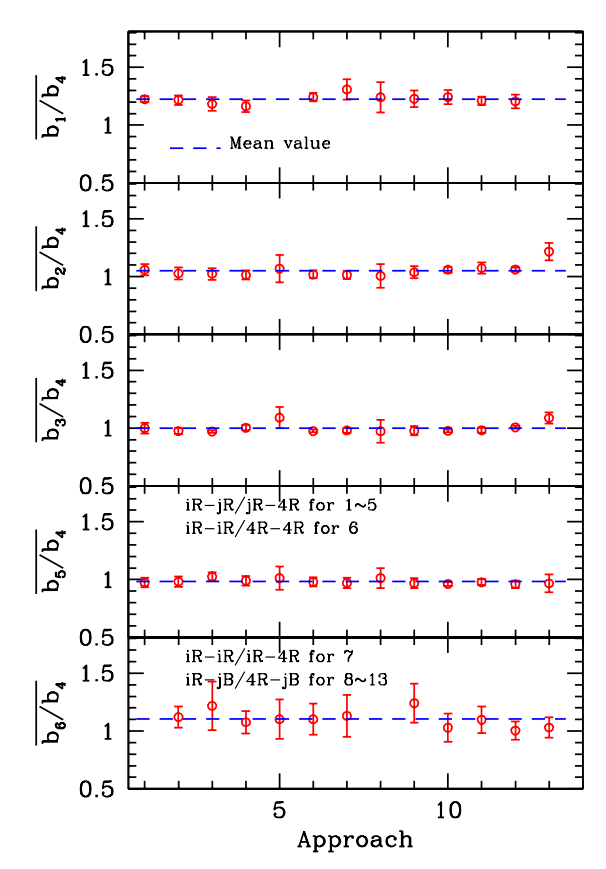


Fig. 12.— The relative bias parameters for red galaxies obtained from the correlation functions over 0.98 $h^{-1}{\rm Mpc}$ to 9.8 $h^{-1}{\rm Mpc}$ using 13 different approaches (see the main text for details). The errorbars are based on the scatter of the data points in the range 0.98 $h^{-1}{\rm Mpc}$ ($r_p \leq 9.8~h^{-1}{\rm Mpc}$). Panels from top to bottom correspond to the bias parameters for Fired (i=1,2,3,5,6), normalized by that of F4red. The horizontal axis labels the different approaches that are used to determine the bias parameter for each subsamples. Some data points are missing, because the redshift overlap between F1 and F6 is too small to measure their cross-correlation function reliably.

 $r_p \gtrsim 1 \, h^{-1} {
m Mpc}$ all correlation functions are roughly parallel, but on smaller scales different galaxies may have different behaviors (see Fig. 5). In order to investigate the scale-dependence of the correlation functions in more detail, we plot in Fig. 15 the ratios between the various projected correlation functions, $W(r_p)$, and a normalization function, $W_0(r_p)$, which is the power-law fit to the projected correlation function of the sample F^* on large scales and corresponds to $r_0 = 5.49 \, h^{-1} {
m Mpc}$ and $\alpha = 1.76$. Three top panels show results for red galaxies; six middle panels show results between red and blue galaxies; and three bottom panels show results for blue galaxies. Based on the figure, we can draw the following conclusions:

- \bullet On scales larger than 1 $h^{-1}{\rm Mpc}$, all the correlation functions are roughly parallel, a fact we have mentioned earlier.
- The cross-correlation functions between the brightest red galaxies and other red galaxies have enhanced clustering on scales smaller than $\sim 1~h^{-1}{\rm Mpc}$, and the enhancement is the strongest for the cross-correlation between the brightest and faintest samples.

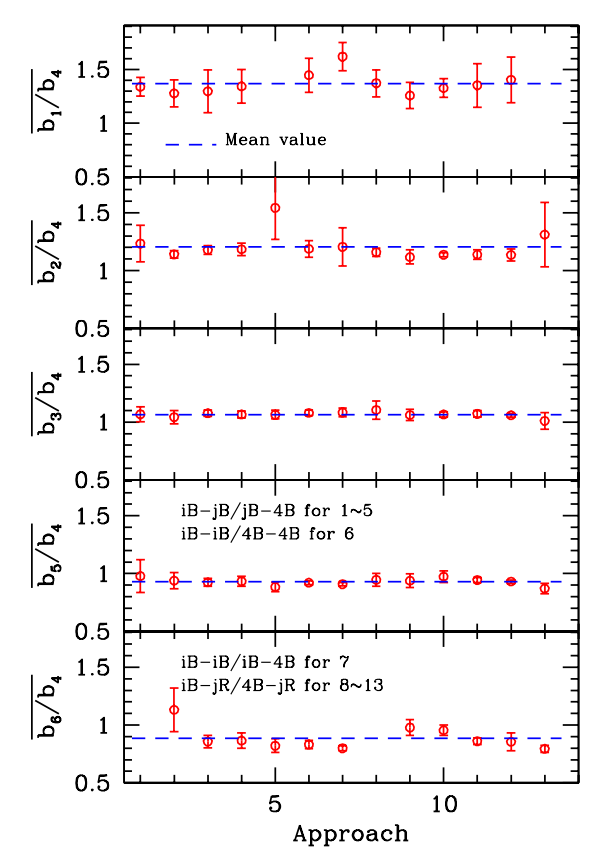


Fig. 13.— The same as Fig. 12 for blue galaxies. Panels from top to bottom correspond to the bias parameters for ${\rm Fi_{blue}}$ (i=1,2,3,5,6), normalized by that of ${\rm F4_{blue}}$.

- The cross-correlation functions among faint blue galaxies, and between faint-blue and faint-red galaxies, appear to be suppressed slightly on scales $\lesssim 1~h^{-1}{\rm Mpc}$ relative to the extrapolations from larger scales.
- The brightest blue galaxies show enhanced correlation with red galaxies of different luminosities on scales $\lesssim 1 \, h^{-1}{\rm Mpc}$.

Some of these results are expected, as it is well known that red galaxies reside preferentially in rich systems, such as clusters and groups, while faint blue galaxies are distributed in the field. Note, however, that the cross-correlation functions between the brightest red galaxies and faint red galaxies are lower than the autocorrelation function of the brightest galaxies on scales $r_p \gtrsim 1 \ h^{-1}{\rm Mpc}$, suggesting that not all faint red galaxies are associated with the brightest red galaxies. There is no enhancement in the cross-correlation functions on small scales between red galaxies and all except the brightest blue galaxies. This again can be explained by the fact that blue galaxies with low and intermediate luminosities are distributed in the field.

One surprising result is that the brightest blue galaxies are strongly correlated with red galaxies on small scales, and in many ways the clustering properties of these galaxies are similar to that of red galaxies with intermediate luminosities. In order to understand this result in more detail, we have examined the properties of this population of galaxies more closely. Using the group catalogue constructed by Yang et al. (2007, in

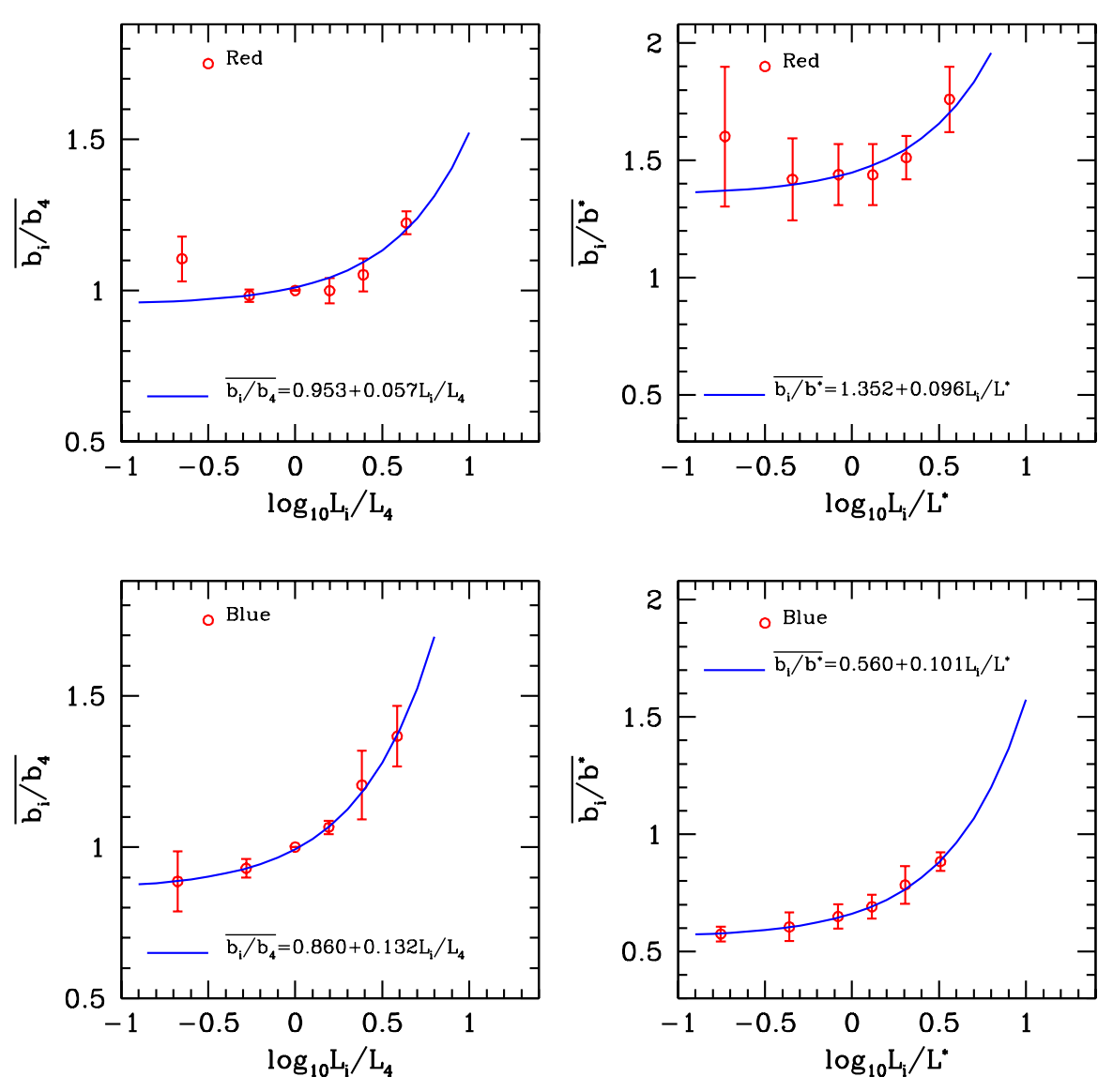


Fig. 14.— Left panels: The average relative bias parameter, obtained using the correlation data in $0.98 \, h^{-1} \mathrm{Mpc} < r_p \le 9.8 \, h^{-1} \mathrm{Mpc}$ as a function of galaxy luminosity, for red (upper panel) and blue (lower panel) galaxies. The results are obtained using the flux-limited samples, and both the bias parameters and the luminosities are normalized by the values of F4_{red} and F4_{blue}, respectively. For a given liminosity, the mean and errorbar are based on the different measurements shown in Figs. 12 and 13. The solid curves show fits to the data. Right panels: The same as the left panels, except that here the bias parameters and the luminosities are normalized by the values for L^* galaxies.

preparation), we find that $\sim 15\%~(\sim 80\%)$ of the brightest blue galaxies are the central galaxies of groups with masses $\gtrsim 10^{13.5}h^{-1}{\rm M}_{\odot}~(\gtrsim 10^{13}h^{-1}{\rm M}_{\odot})$, compared to $\sim 30\%~(\sim 85\%)$ for the red galaxies in the same luminosity bin. It is therefore possible that a fraction of the brightest blue galaxies are in fact 'early-type' galaxies and their relatively blue colors are probably due to rejuvenation of star formation or AGN activities in their centers. Clearly, further analysis is required in order to understand the properties of this population of galaxies in more detail.

Next we discuss how our results may put constraints on the stochasticity/non-linearity in the bias relation. Consider the density field (smoothed on some scale) traced by a population i of galaxies, δ_i . In general we may write it in terms of the density field of another population, δ_j , as

$$\delta_i = B_{ij}\delta_j + f_i(\delta_j) + \epsilon_{ij}, \qquad (13)$$

where the first term on the right-hand side describes the linear part of the correlation between the two populations, the second term is the non-linear part, and ϵ_{ij} is the stochastic, uncorrelated part: $\langle \epsilon_{ij} \delta_j \rangle = 0$. It then follows that

$$\langle \delta_i \delta_j \rangle = B_{ij} \langle \delta_i^2 \rangle + \langle \delta_j f_i(\delta_j) \rangle,$$
 (14)

and

$$\langle \delta_i^2 \rangle = B_{ij}^2 \langle \delta_j^2 \rangle + \langle \epsilon_{ij}^2 \rangle + \langle f_i^2(\delta_j) \rangle + 2B_{ij} \langle \delta_j f_i(\delta_j) \rangle.$$
 (15)

Thus, for any two populations we can define two relative bias factors, one based on the cross correlation with another population, and one based on the auto-correlation functions of the two populations:

$$B_{ij}^{(c)} \equiv \frac{\langle \delta_i \delta_j \rangle}{\langle \delta_j^2 \rangle}; \tag{16}$$

$$B_{ij}^{(a)} \equiv \left(\frac{\langle \delta_i^2 \rangle}{\langle \delta_j^2 \rangle}\right)^{1/2}.$$
 (17)

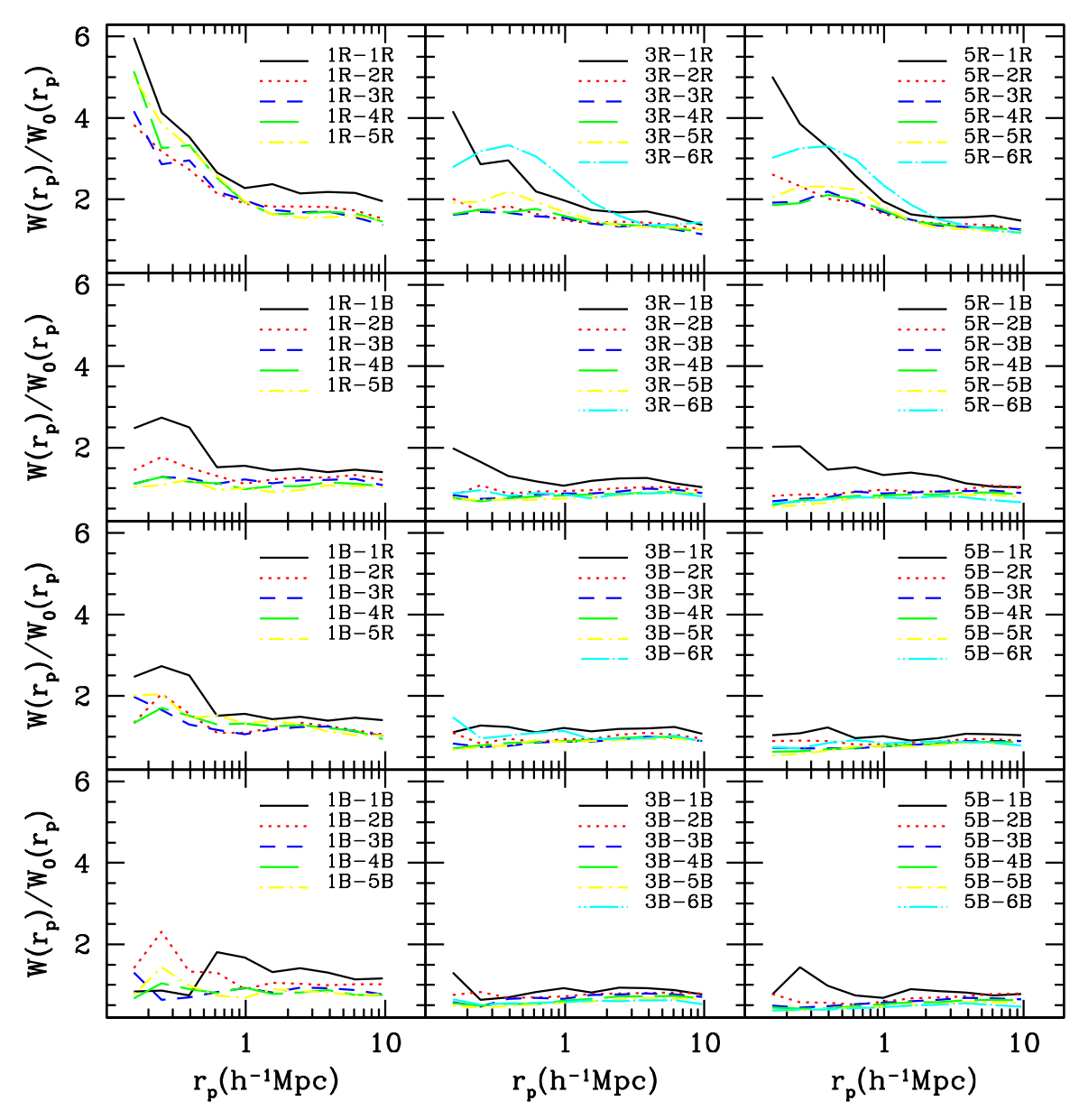


Fig. 15.— The ratios between the projected correlation function $W(r_p)$ and $W_0(r_p)$ for cases with various combinations of color and luminosity, where $W_0(r_p)$ is the power-law fit to the projected correlation function of sample F^* on large scales ($r_0 = 5.49 \ h^{-1} \mathrm{Mpc}$, $\alpha = 1.76$). Three top panels show the results for red galaxies, six middle panels show the results between red and blue galaxies, and three bottom panels show the results for blue galaxies. In each panel, iR-jR denotes $\mathrm{Fi}_{\mathrm{red}}$ with $\mathrm{Fj}_{\mathrm{plue}}$, iB-jB denotes $\mathrm{Fi}_{\mathrm{blue}}$ with $\mathrm{Fj}_{\mathrm{blue}}$.

The square of the ratio between these two bias factors is

$$\mathcal{R}_{ij} \equiv \left(\frac{B_{ij}^{(a)}}{B_{ij}^{(c)}}\right)^2 = \frac{\langle \delta_i^2 \rangle \langle \delta_j^2 \rangle}{\langle \delta_i \delta_j \rangle^2} \\
= 1 + \frac{\langle \epsilon_{ij}^2 \rangle + \zeta_{ij}}{\langle \delta_i \delta_j \rangle^2 / \langle \delta_i^2 \rangle}, \tag{18}$$

where

$$\zeta_{ij} \equiv \langle f_i^2(\delta_j) \rangle - \langle \delta_j f_i(\delta_j) \rangle^2 / \langle \delta_j^2 \rangle$$
 (19)

describes the contribution due to the non-linear part of the relative bias relation. Note that both the stochastic component, $\langle \epsilon_{ij}^2 \rangle$, and the non-linear component, ζ_{ij} , can cause \mathcal{R}_{ij} to deviate from 1, and in general it is difficult to separate these two components. On large scales where the non-linear component in the bias relation may be neglected, we have

$$\mathcal{R}_{ij} = 1 + \frac{\langle \epsilon_{ij}^2 \rangle}{B_{ij}^2 \langle \delta_i^2 \rangle}.$$
 (20)

To examine the importance of stochasticity/nonlinearity in the relative bias relations, we calculate \mathcal{R}_{ij} for galaxies of different luminosities and colors. Based on equation (18), we estimate \mathcal{R}_{ij} using

$$\mathcal{R}_{ij} = \frac{W_{ii}W_{jj}}{W_{ij}^2}, \qquad (21)$$

where W_{ii} and W_{jj} are the auto-correlation functions of subsamples 'i' and 'j', respectively, and W_{ij} is the cross-correlation function between the two subsamples. Note

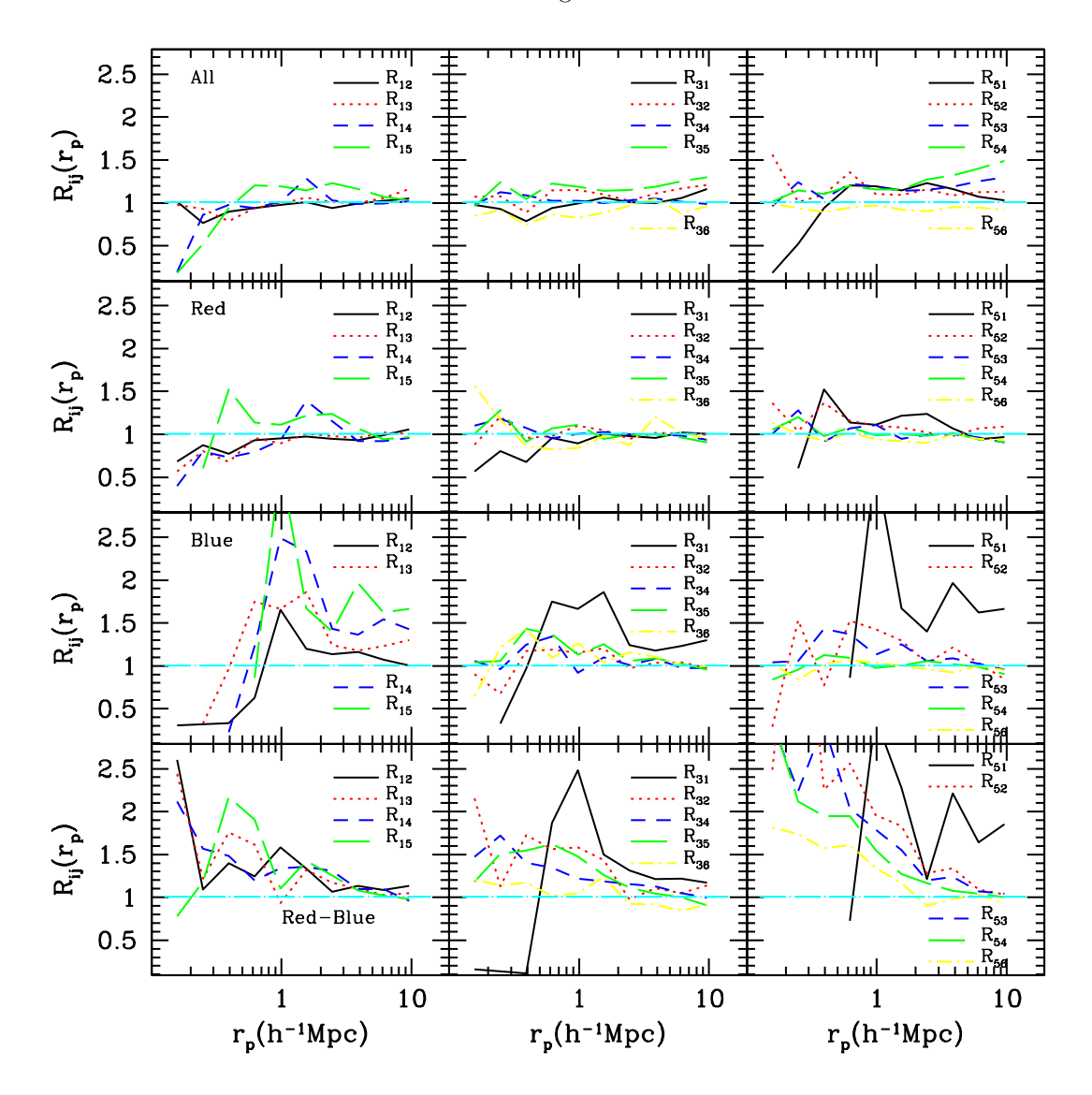


FIG. 16.— The value of \mathcal{R}_{ij} as a function of r_p for cases with various combinations of color and luminosity. Panels from top to bottom show results for all-all, red-red, blue-blue, and red-blue samples, respectively. The straight line in each panel shows $\mathcal{R}_{ij} = 1$.

that 'i' and 'j' denote not only luminosity samples but also color samples. Unlike what we did above, here we estimate W_{ii} , W_{jj} and W_{ij} all in the overlapping region of the two samples in question, so that volume effects are minimized.

In Fig 16 we show \mathcal{R}_{ij} as a function of r_p for various combinations of color- and luminosity-samples. The results are quite noisy in some cases, again because of the small overlap of the samples involved. As one can see, for cases where \mathcal{R}_{ij} is well determined, it is close to 1 for all-all and red-red pairs of samples. For blue-blue pairs, \mathcal{R}_{ij} is also close to 1 except the cases involving the brightest galaxies where \mathcal{R}_{ij} can be significantly larger than 1. As we have discussed above, the brightest blue galaxies have clustering properties different from that of fainter blue galaxies, because a significant fraction of them are, like bright red galaxies, central galaxies of relatively massive groups. For red versus blue galaxies, \mathcal{R}_{ij} is significantly larger than 1 on small scales. The signal is also more prominent between faint red and faint blue galaxies and

can extend to a few h^{-1} Mpc.

To show this more clearly, we plot the average value of \mathcal{R}_{ij} over two different scales. The results are shown in Figs. 17 – 18 for all versus all, red versus red, blue versus blue, and red versus blue, respectively. In all the figures, circles show results based on clustering on large scales $(0.98\ h^{-1}\mathrm{Mpc} \le r_p \le 9.6\ h^{-1}\mathrm{Mpc})$, while crosses show results based on clustering on small scales $(0.16\ h^{-1}\mathrm{Mpc} \le r_p \le 0.98\ h^{-1}\mathrm{Mpc})$. As one can see, on large scales $(\gtrsim 1\ h^{-1}\mathrm{Mpc})\ \mathcal{R}_{ij}$ is very close to 1 for redred, blue-blue (with the exception of cases involving the brightest blue galaxies), and all-all pairs, but has a value between 1.2 to 1.4 for pairs between faint red and blue galaxies. On scales $\lesssim 1\ h^{-1}\mathrm{Mpc}$, the ratio is again very close to 1 for all-all, red-red and blue-blue pairs, but is significantly larger than 1 for red versus blue galaxies and is as large as ~ 2 for faint-red versus faint-blue galaxies.

These results suggest that red (or blue) galaxies of different luminosities trace each other almost linearly and in an almost deterministic way on both small and

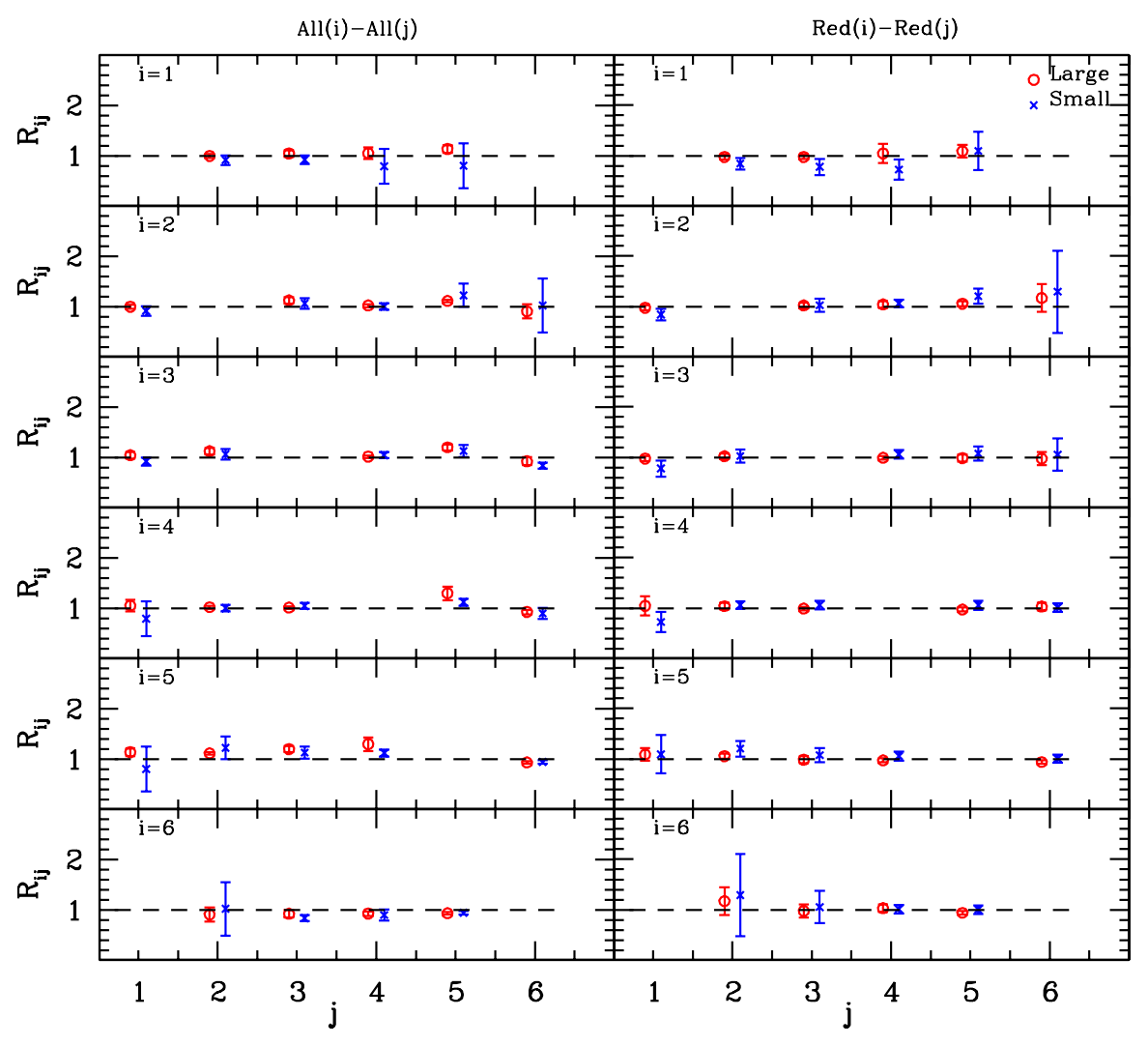


Fig. 17.— The ratio \mathcal{R}_{ij} defined in equation (18) for all (left panels) and red (right panels) galaxies. In all panels, circles show results based on data on large scales, $0.98 \ h^{-1}\mathrm{Mpc} \le r_p \le 9.6 \ h^{-1}\mathrm{Mpc}$, while crosses show results based data on small scales, $0.16 \ h^{-1}\mathrm{Mpc} \le r_p \le 0.98 \ h^{-1}\mathrm{Mpc}$. From top to bottom are results for i=1,2,3,4,5,6, respectively. The value of j for each case is labelled on the horizontal axis. The dashed line in each panel shows $\mathcal{R}_{ij}=1$. The errorbars are estimated using the scatter of the data points on large scales $0.98 \ h^{-1}\mathrm{Mpc} \le r_p \le 9.6 \ h^{-1}\mathrm{Mpc}$ and small scales $0.16 \ h^{-1}\mathrm{Mpc} \le r_p \le 0.98 \ h^{-1}\mathrm{Mpc}$, respectively.

large scales, but there is a significant stochastic/nonlinear component in the relationship between red and blue galaxies of different luminosities, and in particular on small scales. The large value of R_{ij} on small scales between red and blue galaxies (except the brightest blue galaxies) is almost certainly due to the fact that blue galaxies of low and intermediate luminosities avoid dense groups and clusters while red galaxies reside preferentially in such places. The fact that such stochastic/nonlinear component extends to a few h^{-1} Mpc (see Fig. 16) suggests that the clustering of clusters and groups on large scales may produce segregation of the galaxy populaion on large scales.

7. SUMMARY

In this paper, we use galaxy samples constructed from the SDSS Data Release 4 (DR4) to study the cross-correlation functions between galaxies with different luminosities and colors. Galaxies are separated at $g-r=-0.7-0.032(M_{r,0.1}+16.5)$ into red and blue samples according their colors, and each of the color samples

is further divided into 6 subsamples according to luminosity. We measure the projected two-point correlation function for each subsample, and the projected cross-correlation for each pair of subsamples. Each correlation function is fitted with power laws over two different ranges of separations: $0.98 \ h^{-1}{\rm Mpc} \le r_p \le 9.6 \ h^{-1}{\rm Mpc}$ and $0.16 \ h^{-1}{\rm Mpc} \le r_p \le 0.98 \ h^{-1}{\rm Mpc}$, and each of the power laws are characterized by a correlation length, r_0 , and a logarithmic slope, α . Our main results can be summarized as follows:

- 1. At projected separations $r_p \gtrsim 1 \, h^{-1} {\rm Mpc}$, all correlation functions are roughly parallel to each other, but on smaller scales different populations of galaxies have different behaviors.
- 2. The auto- and cross-correlation functions of red galaxies on $r_p \lesssim 1 \ h^{-1}{\rm Mpc}$ are significantly enhanced relative to those on larger scales. The effect is the strongest between the brightest red galaxies and other red galaxies. Such enhancement is absent for blue galaxies and in the cross-correlation

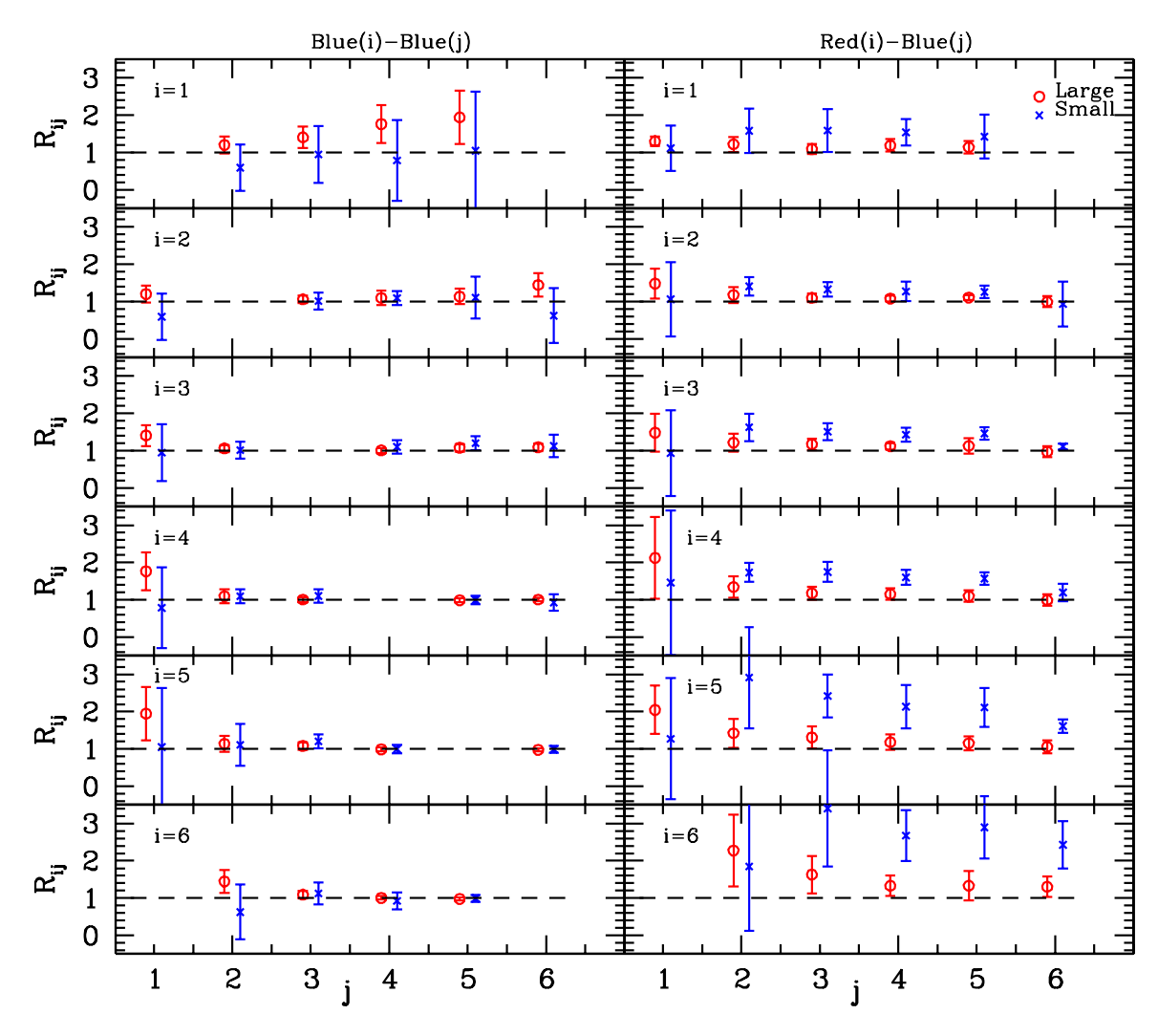


Fig. 18.— The same as Fig. 17, but here results are shown for blue versus blue galaxies (left panels) and red versus blue galaxies (right panels).

between red and blue galaxies.

- 3. For blue galaxies the luminosity-dependence of the correlation amplitude on large scales is strong over the entire luminosity range, while for red galaxies the dependence is weaker and becomes insignificant for luminosities below L^* . There is indication that the luminosity-dependence may inverse at the faint end.
- 4. For a given luminosity, red galaxies are more strongly clustered than blue galaxies on both large and small scales, and the difference is larger for fainter luminosities.
- 5. One large scale, the bias factors of a given population of galaxies obtained from its cross correlations with other populations of galaxies are similar, and comparable to that based on the auto-correlation function.
- 6. On both large and small scales, the ratio \mathcal{R}_{ij} is very close to 1 for red (or blue except the brightest) galaxies of different luminosities, suggesting that the bias relations between red (or blue) galaxies

of different luminosities are close to be linear and deterministic.

- 7. On scales $\lesssim 1 h^{-1}$ Mpc, R_{ij} is significantly larger than 1 between red and blue galaxies and as large as ~ 2 between faint red and faint blue galaxies, suggesting that a significant stochastic/non-linear component exists in the bias relations between blue and red galaxies on small scales.
- 8. The clustering properties of the brightest blue galaxies resemble more that of red galaxies of intermediate luminosities than that of fanter blue galaxies, indicating that a significant fraction of them are located in relative rich systems.

The results obtained in this paper provide important information about the relationships between the spatial distributions of galaxies of different properties in space. To explore the implications of our findings for galaxy formation in the cosmic density field, the results obtained here should be combined with semi-analytical and/or halo occupation models to constrain how galaxies populate dark matter halos, and how galaxies are distributed

in individual dark matter halos. We will come back to this in the future.

After finishing our paper, we noticed that Swanson et al. (2007) has carried out a similar investigation to study the relative bias for galaxies of different luminosities and colors, using a counts-in-cells analysis. Our results are qualitatively the same as theirs, but a detailed comparison between the two analyses is difficult because of the differences in the statistical methods and sample selections.

We thank Cheng Li for the help in understanding the SDSS data. XY is supported by the One Hundred Talents project of the Chinese Academy of Sciences and grants from NSFC (Nos.10533030, 10673023). HJM would like to acknowledge the support of NSF AST-0607535, NASA AISR-126270 and NSF IIS-0611948.

Funding for the SDSS and SDSS-II has been provided by the Alfred P. Sloan Foundation, the Participating Institutions, the National Science Foundation, the U.S. Department of Energy, the National Aeronau-

tics and Space Administration, the Japanese Monbukagakusho, the Max Planck Society, and the Higher Education Funding Council for England. The SDSS Web Site is http://www.sdss.org/. The SDSS is managed by the Astrophysical Research Consortium for the Participating Institutions. The Participating Institutions are the American Museum of Natural History, Astrophysical Institute Potsdam, University of Basel, Cambridge University, Case Western Reserve University, University of Chicago, Drexel University, Fermilab, the Institute for Advanced Study, the Japan Participation Group, Johns Hopkins University, the Joint Institute for Nuclear Astrophysics, the Kavli Institute for Particle Astrophysics and Cosmology, the Korean Scientist Group, the Chinese Academy of Sciences (LAMOST), Los Alamos National Laboratory, the Max-Planck-Institute for Astronomy (MPIA), the Max-Planck-Institute for Astrophysics (MPA), New Mexico State University, Ohio State University, University of Pittsburgh, University of Portsmouth, Princeton University, the United States Naval Observatory, and the University of Washington.

REFERENCES

Adelman-McCarthy J. K., Agüeros M. A., Allam S. S., Anderson K. S. J., Anderson S. F., Annis J., Bahcall N. A., Baldry I. K., et al., 2006, ApJS, 162, 38

Baldry I.K., Glazebrook K., Brinkmann J., Ivezić Ž., Lupton R.H.,

Baldry I.A., Glazebrook K., Brinkmann J., Ivezic Z., Lupton R.H., Nichol R.C., Szalay A.S., 2004, ApJ, 600, 681

Bell E.F., et al., 2004, ApJ, 608, 752

Benoist, C., Maurogordato, S., da Costa, L. N., Cappi, A., & Schaeffer, R. 1996, ApJ, 472, 452

Berlind A. A., Weinberg D. H., 2002, ApJ, 575, 587

Blanton M. R., Brinkmann J., Csabai I., Doi M., Eisenstein D., Fukugita M., Gunn J. E., Hogg D. W., et al., 2003a, AJ, 125, 2248

Blanton M. R., Hogg D. W., Bahcall N. A., Brinkmann J., Britton M., Connolly A. J., Csabai I., Fukugita M., et al., 2003b, ApJ, 592, 819

Blanton M. R., et al., 2003c, ApJ, 594, 186 Blanton M. R., et al., 2005, AJ, 129, 2562 Brown, M. J. I., Webster, R. L., & Boyle, B. J. 2000, MNRAS, 317,

Börner, G., Mo, H., & Zhou, Y. 1989, A&A, 221, 191 Budavari, T., et al., 2003, ApJ, 595, 59 Cooray A., Sheth R., 2002, PhR, 372, 1 Davis, M., Peebles, P.J.E. 1983, APJ 267,465 Guzzo, L., Strauss, M. A., Fisher, K. B., Giovanelli, R., & Haynes,

Guzzo, L., Strauss, M. A., Fisher, K. B., Giovanein, R., & Haynes, M. P. 1997, ApJ, 489, 37
Goto, T., Yamauchi, C., Fujita, Y., Okamura, S., Sekiguchi, M., Smail, I., Bernardi, M., & Gomez, P. L. 2003, MNRAS346, 601
Hamilton, A. J. S. & Tegmark, M. 2004, MNRAS, 349, 115
Hogg D.W., et al., 2004, ApJ, 601, L29
Jing, Y. P., Mo, H. J., & Boerner, G. 1991, A&A, 252, 449
Jing, Y. P., Mo, H. J., & Börner, G. 1998, ApJ, 494, 1

Li, C., Kauffmann, G., Jing, Y.P., White, S. D. M., Boerner, G., Cheng, F.Z. 2006, MNRAS368, 21 Loveday, J., Maddox, S. J., Efstathiou, G., & Peterson, B. A. 1995, ApJ, 442, 457

ApJ, 442, 437
Madgwick, D. S. et al. 2003, MNRAS, 344, 847
Norberg, P., et al. 2001, MNRAS, 328, 64
Norberg, P., et al. 2002, MNRAS, 332, 827
Park, C., Vogeley, M. S., Geller, M. J., & Huchra, J. P. 1994, ApJ, 431, 569

Peacock J. A., Smith R. E., 2000, MNRAS, 318, 1144
Peebles, P.J.E. 1980, The Large-Scale Structure of the Universe, Princeton University Press, Princeton
Seljak U., 2000, MNRAS, 318, 203
Swanson M.E.C., Tegmark M., Blanton M., Zehavi I., 2007, preprint (astro-ph/0702584)
van den Bosch, F. C., Yang, X., Mo, H. J., , 2003, MNRAS, 340, 771

Weinmann, S.M., van den Bosch, F. C., Yang, X.H., Mo, H. J., Croton, D. J., Moore, B., 2006, MNRAS, 366, 2 Willmer, C. N. A., da Costa, L. N., & Pellegrini, P. S. 1998, AJ,

115, 869 Yang, X., Mo, H. J., van den Bosch, F. C., 2003, MNRAS, 339, 1057

Yang, X., Mo, H. J., van den Bosch, F. C., Weinmann, S.M., C., Li, Y.P., Jing, 2005, MNRAS, 362, 711

York, D. G., et al., 2000, AJ, 120, 1579

Zehavi, I., et al., 2005, ApJ, 571, 172 Zehavi I., et al., 2005, ApJ, 630, 1